FRACTURE IN DISORDERED BRITTLE MEDIA

A Dissertation

Presented to the Faculty of the Graduate School

of Cornell University

in Partial Fulfillment of the Requirements for the Degree of

Doctor of Philosophy

by

Ashivni Shekhawat

May 2013

FRACTURE IN DISORDERED BRITTLE MEDIA

Ashivni Shekhawat, Ph.D.

Cornell University 2013

This thesis consists of three main chapters, an introduction, and an appendix. The introduction (chapter 1) gives a general historical introduction to the problem of brittle fracture in disordered media. Chapters 2 and 4 are concerned with various aspects of fracture in disordered fuse networks. Chapter 2 investigates the asymptotic properties of fracture strength distributions, and explores their relation with extreme value statistics. Chapter 4 deals with critical phenomena in brittle fracture. This chapter introduces the concept of finite-sized criticality as a means to explain how fracture can have mixed properties of abrupt and continuous phase transitions. Chapter 3 describes the collective dynamics at the non equilibrium metal insulator transition. The phenomenon of dielectric breakdown at the metal insulator transition shares several characteristics with fracture, and provides a suitable build up to the development presented in chapter 4.

The first three parts of the appendix provide an introduction to the various mathematical tools required in order to better appreciate the content of this thesis. Appendix A.1 discusses the basics of extreme value theory, while A.2 and A.3 provide a light introduction to linear elastic fracture mechanics. Appendix A.4 summaries some results on crack propagation in graphene that are not sufficiently well developed to merit a chapter, and yet are developed enough to merit a mention.

BIOGRAPHICAL SKETCH

Ashivni Shekhawat was born and brought up in India by loving parents, Col. S. S. Shekhawat and Mrs. Poonam Shekhawat. He was awarded a Bachelors of Technology degree in Aerospace Engineering by the Indian Institute of Technology Kanpur in 2004. He obtained a Masters of Science degree in Aerospace Engineering from the Texas A&M University in 2008.

To my parents, my teachers, and Preetha.

ACKNOWLEDGEMENTS

I acknowledge the help, support, and guidance of my advisor, Prof. James P. Sethna, with the utmost gratitude. He helped me become a better scientist and a better human. I am indebted to all my teachers, particularly, Mrs. Anuradha Prasad, Mr. Trivedi, Prof. C. S. Upadhaya, Prof. N. Ananthkrishnan, Prof. J. Hurtado, Prof. S. L. Phoenix, Prof. S. Resnick, Prof. R. Hennig and Prof. S. Zapperi for their enthusiasm and confidence in me.

I am eternally indebted to my mother, Poonam Shekhawat, and my father, Col. S. S. Shekhawat, for their love, encouragement, and wisdom. My sisters – Alka Gohil and Aarti Jadhon – made my childhood memorable, and have been rock-solid in their support and love since then; for this I am deeply grateful. Finally, I would like to thank Preetha – the joy and soul of my life.

I acknowledge the financial support provided by the US DOE via the grant DOE-BESDE-FG02-07ER46393. Some of the numerical work was carried out by using the resources provided by the National Science Foundation through TeraGrid under grand number TG-DMR100025.

TABLE OF CONTENTS

LIST OF FIGURES

CHAPTER 1

INTRODUCTION

This is a thesis about *fracture* or how and why things break. Fracture, or the act of breaking of an object, is more important in our lives than we might think. A violent fracture in earth's crust can lead to terrible earthquakes, while slow creep in earth's crust leads to the formation of mountain ranges and migration of entire continents. Uncontrolled crack growth and fracture can lead to dangerous industrial accidents, while controlled fracture and removal of material is central to all metal working and several other industrial processes. In fact, one of the central technological challenges of our civilization is to make materials with superior strength and fracture characteristics.

This thesis is primarily concerned with statistical models of fracture, the only exception being appendix A.4, which discusses criteria for crack path prediction. The goal of this chapter is to provide a brief literature and historical review, and to discuss the scope of this thesis and make clear the problems that it tries to address. Throughout this thesis it is assumed that the reader has a basic level of familiarity with concepts of probability, statistics, extreme value statistics, linear elasticity, linear elastic fracture mechanics, critical phenomena and the renormalization group. There are a great many references and books that the reader might use to gain an adequate knowledge of these topics; I would suggest reading the book by Sheldon and Ross on probability [1], the book by Casella and Berger on statistical inference [2], the book by Resnick [3] and the book by Leadbetter *et al.* [4] on extreme value statistics, the book by Zehnder [5] and the book by Gross and Thomas [6] on fracture mechanics, and the books by Cardy [7] and Sethna [8] on critical phenomena and the renormalization group.

Appendix A.1 gives a very brief introduction to some important results in extreme value statistics, and appendix A.2 gives a brief introduction to linear elastic fracture mechanics.

1.1 Literature and Historical Review

The subject of fracture and failure in materials is very broad and has been developed by several different communities. The continuum theory of fracture, or linear elastic fracture mechanics (LEFM), has occupied the center stage in the development of this discipline. LEFM has been extended to include plasticity, nonlinearity, and dynamic effects. Indeed, most of the industrial safety and fracture related design is based on principles of LEFM. More recently, the availability of sophisticated computers and experimental equipment has enabled the study of fracture at scales smaller than the continuum scale. Computer simulations have shed light on the molecular level mechanisms of fracture. These simulations have also illuminated several interesting phenomena that are hard to study experimentally, such as the dissipative processes at the atomic scale, fractal like roughness of fracture surfaces (measured by, for example, a roughness exponent, see Ref. [9]), and the dynamic crack tip instability. Recent developments in density functional theory have started to enable first principle studies of fracture, a field that I believe will be very exciting as it develops and matures.

Historically, statistical models of fracture have not been studied in mainstream fracture mechanics. These models have been largely developed by statisticians and statistical physicists. The fiber bundle and the fuse network are the two most prominent statistical models of fracture. The fiber bundle has been

Figure 1.1: A reproduction of Leonardo da Vinci's experimental apparatus for testing the tensile strength of wires of varying length and thickness, based on his drawings in his notebook *Codex Atlanticus*, sheet 222 1486-1490. The apparatus consists a container to hold sand, and pour it slowly into a bucket suspended by a wire. The weight of sand at which the wire broke would characterize the strength of the wire. Image copyright: 2013 Museo Nazionale della Scienza e della Tecnologia "Leonardo da Vinci" all rights reserved.

studied for almost a century now, however the study of fuse networks proliferated only after the advent of fast computers. These models have greatly improved our understanding of the interplay between disorder and fracture, a subject where LEFM is most lacking. I will review the literature and development of LEFM and the statistical models of fracture in the next few sections of this chapter.

Historically, the first documented studies of fracture are perhaps due to

Leonardo da Vinci. In his experiments da Vinci used a device similar to the one depicted in figure 1.1. The device would load metallic wires slowly, allowing da Vinci to note the weight of sand that the wire broke at. He observed that shorter wires were stronger, which was perhaps the first scientific study of the "smaller is stronger" size effect.

The modern development of fracture mechanics has been largely motivated by practical industrial applications. In 1920, A. A. Griffith of the Royal Aircraft Establishment [10], developed a theory of fracture in brittle materials in order to understand the effect of surface treatment on the strength of metallic machine parts subject to repeated loading. Even though the subject of repeated loading, or fatigue, is not understood in detail even today, the theory of brittle fracture is well established, and has not changed substantially in spirit from what Griffith proposed. In 1926 F. T. Peirce [11] studied the strength of 'fiber bundles' in order to understand the strength related properties of cotton yarns and other related materials. The work of Peirce has developed into the field of statistical models of fracture, and the fiber bundle is still an active topic of research. The research for understanding the fracture properties of specific material systems was perhaps accelerated in a large measure by the developments surrounding the Liberty Ships in the World War II. Figure 1.2 shows the S S Schenectady, one of the several Liberty Ships that suffered catastrophic failure due to unexpected hull fracture. It was later discovered that the incidents were due to the embrittlement of low grade steel in icy waters. Fracture mechanics is thus a most interesting field, its history rich with lore, and its theory deep, and yet evolving.

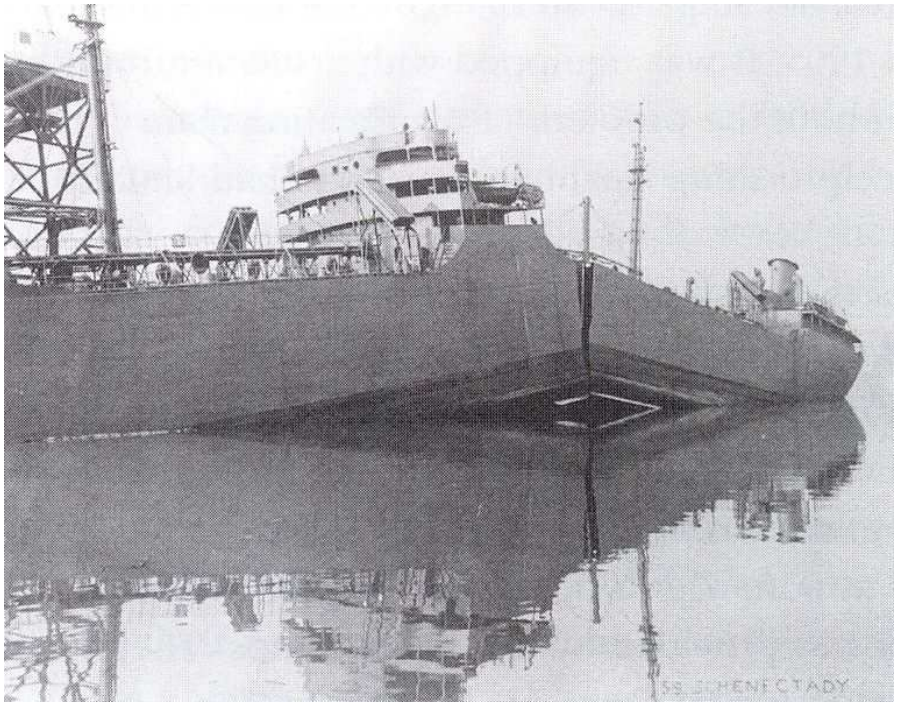

Figure 1.2: The S S Schenectady was a T2-SE-A1 tanker built during World War II. During its maiden voyage into the Pacific ocean, its hull cracked into two.

1.1.1 Continuum Fracture Mechanics

The modern theory of fracture mechanics began with a landmark paper written by C. E. Inglis in 1913 [12]. Inglis derived an analytical solution for the state of stress in a plate with an elliptical hole. He used the limit of thin ellipses to investigate the behavior of sharp cracks and observed the characteristic stress concentrations at the tip of the thin ellipses. He also noticed the characteristic $1/\sqrt{r}$ singularity at the crack tip. In 1920 Griffith used the Inglis solution to derive a thermodynamic criteria for crack propagation in brittle materials. This criteria has since been called the Griffith criteria for crack propagation. Griffith argued that if the net potential energy of the system decreased by increasing the crack size, then the crack growth would be energetically favorable

and spontaneous. By using the Inglis solution to do exact calculations, Griffith found that the stress needed to grow a defect of length $2a$ was proportional to $\sqrt{\gamma Y/a}$, where γ is the energy need to create a unit area of material surface, and Y is the generalized modulus of elasticity. This result has been a cornerstone of fracture mechanics, and is derived in some detail in appendix A.3. The next major development in LEFM is due to H. M. Westergaard, who in 1939 solved the exact problem of a crack in an elastic material by using the theory of analytic functions [13] ; his approach is discussed in appendix A.2. Westergaard's solutions were 'better' than the Inglis solution insomuch as they did not approximate a sharp crack with a thin ellipse, but rather developed the mathematics needed to deal with the sharp crack singularity. Westergaard used a formulation of elasticity wherein any stress state could be represented by the means of two analytic functions or potentials. Later, Muskhelishvili [14] made some improvements to the potential functions that had some technical advantages over the representation used by Westergaard. In 1957 Irwin wrote a landmark paper where he introduced the celebrated "K-field" concept [15]. These and other ideas were developed by him and Eshelby in a series of related papers around that time [16–21]. The ideas of cohesive zone models of fracture were soon introduced in the works of Dugdale and Barenblatt [22, 23], and have since been used extensively, particularly in FEM modeling [24–35]. Most of the development so far dealt only with linear elasticity. This deficiency was overcome to some extent by the formulation of the so-called J-integral by J. R. Rice [36, 37], which produced a path-independent integral valid for linear as well as nonlinear material behavior. Even though this formulation is generally attributed to Rice, it was derived earlier by Eshelby [19]. The theory of LEFM was well established in its modern form by the late 1960's to the early 1970's, and has changed

only incrementally since then. It is worth mentioning that another approach to modeling cracks is by the use of a continuous distribution of dislocations [38]. This approach has been developed and used by several authors to calculate the energy release rates of kinked or branched cracks [39,40].

No summary of fracture mechanics can be complete without the mention of the fascinating phenomena in dynamic fracture [41–46]. Even though this thesis does not address any questions related to dynamic effects, I provide a brief history of the field for the interested reader. In 1948 N. F. Mott provided the first framework for including inertial effects in fracture [47,48]. He realized that inertial effects can become significant at the high speeds that cracks propagate at. He assumed that cracks reached a steady state, and provided an analysis for this state. In 1951 Yoffe wrote about the dynamics of a moving crack in an elastic medium [49]. Around the same time Irwin used his K-field concept to analyze dynamic fracture [15,16,50]. Irwin realized the key fact that the contribution of surface energy to the resistance to fracture in metals is much smaller than the resistance due to plastic effects. This plays a particularly important role in dynamic fracture since a crack needs a lot more energy to propagate stably in presence of dissipation due to plastic effects. Hall conducted a series of experiments on metals that proved that the dominant mechanism that resisted fracture in metals was indeed plasticity [51]. This idea was used by Orowan to propose a fracture criteria for steels [52]. Wells and others developed photoelastic techniques that helped in generating experimental data for dynamic effects [53–55]. More recently, Chandra and Knauss investigated the dynamics of propagating cracks in a series of papers published in 1984 [56–59]. They observed the well known crack branching instability, which was further studied in a series of experimental and computational papers by Marder, Fineberg and

co-workers [60–71]. Ramanathan [72–74] and Bouchaud [75] have attempted to explain the properties of dynamic fracture, such as crack surface roughening, by using a renormalization group and statistical mechanics based approach. The subject of dynamic fracture, particularly the crack tip instability, is not understood well and remains an open topic for research.

It is an interesting question whether the prediction of crack paths is in the scope of LEFM. In a crystalline material crack growth happens at the atomic scale, and the processes leading to crack growth are inside the nonlinear process zone almost by definition. Thus, it is expected that continuum theories will not have the power to predict the direction of crack growth unless there is an emergent symmetry or a very large correlation length in the problem. This argument not withstanding, several "principles" for crack growth have been suggested. The most celebrated of these is the principle of local symmetry. The other principles include the principle of maximum energy release rate, the principle of maximum hoop stress, and the principle of minimum strain energy density. Griffith-type arguments claim that cracks propagate along the cleavage plane with the minimum surface energy; however, BCC iron cleaves along the $\{100\}$ plane even though at $1000^{\circ}C$ both the $\{111\}$ and $\{110\}$ planes have lower surface energy [76]; similar effects have been observed in numerical simulations as well [77]. It has also been speculated that anisotropy in linear [78] or nonlinear [77] elastic constants can determine the direction of crack growth; in the second case, later work using a potential tuned to isotropic nonlinear elasticity showed the same anomalous behavior [79]. Furthermore, even on a given plane, there is significant anisotropic dependence of the crack growth direction [80,81]. Several authors have either calculated the crack path by assuming local symmetry or maximum energy release [39, 82–88]. Sethna and Hodgdon have showed

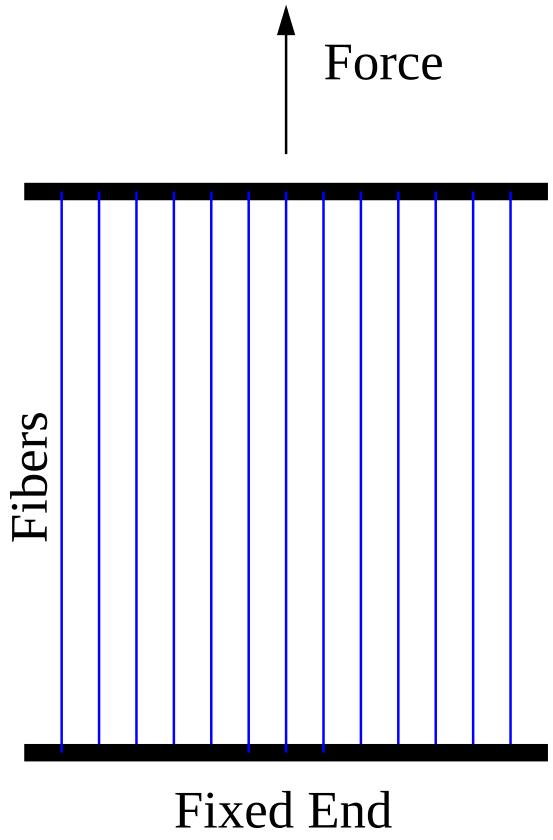

Figure 1.3: A fiber bundle.

that in absence of crystalline anisotropy, symmetry arguments alone imply that after a quick transient, the growth direction aligns with the direction of local symmetry [89]. However, none of the criteria give consistent predictions for crystalline materials. In this thesis I will study some aspects of crack propagation in graphene, a two dimensional crystalline material, by using molecular dynamics simulations. I will interpret the results in the framework of the various theories mentioned earlier.

1.1.2 Statistical Models

The treatment of fracture in the linear elastic theory assumes that the crack exists in an otherwise homogeneous material. This is not always the case, as real materials have defects and disorder. While there have been efforts to model disorder within elastic theory, the statistical models of fracture provide a much more elegant approach. F. T. Peirce introduced the first such model in his studies of cotton yarns and other textile oriented materials [11]. His model has since been called the fiber bundle model. The model essentially considers a bundle of fibers that have been clamped at both ends and are subjected to increasing load (or extension, see Fig. 1.3). The individual fibers have a strength that is drawn from a known distribution. The dynamics of failure of the bundle and the distribution of this strength are the topic of study. The dynamics and distribution of strength vary widely with the load sharing rule. The simplest rule is perhaps the democratic load sharing. In this rule when a fiber breaks, its load is distributed uniformly over all surviving fibers. Thus, at any given time all fibers support the same amount of load. In 1945 H. E. Daniels proved that for the democratic fiber bundle the asymptotic distribution of strength (for large number of fibers) is given by a Gaussian distribution [90]. The local load sharing rules mimic the stress concentration effects better. In such rules when a fiber breaks, its load is distributed in some manner over its neighbors, say each nearest neighbor takes half the load or each two nearest neighbors take fourth the load, etc. In a series of papers beginning in the early 1970's S. L. Phoenix and co-workers have produced a series of mathematically rigorous results for the distribution of failure strength for various local load sharing rules [91–101]. Harlow and Phoenix introduced a transition matrix approach, which was used later by Duxbury and Leath to formulate an eigenvalue problem to study the strength distribution of a

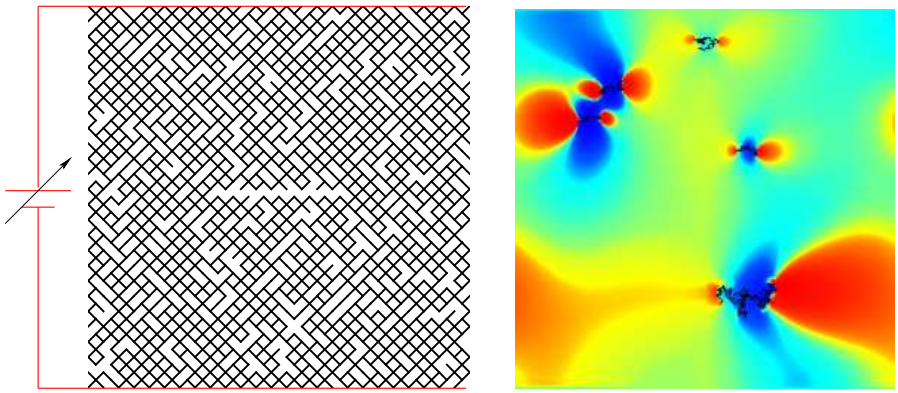

Figure 1.4: (Left) A disordered fuse network with some fuses removed at random. The fuse network has a distinguishable 'crack' in the center. (Right) The current distribution in a fuse network with a few flaws (not the same as the fuse network shown on the left). Notice the stress concentrations at the crack tips and the long ranged stress fields of the cracks.

class of related models asymptotically [102]. It is interesting to note that almost all exact results indicate an logarithmic size effect, i.e., the mean failure stress $\langle\sigma\rangle$ decays logarithmically with the size of the bundle L, or $\langle\sigma\rangle \sim 1/(\log L)^{\alpha}$ ($\alpha = 2$ for the randomly diluted fuse network, see Chapter 2, Fig. 2.3). The review paper [103] and the references therein discuss several aspects of the fiber bundle model in much greater detail.

One of the greatest criticisms of the fiber bundle model is its lack of realistic physics in load redistribution. Fracture in real materials is mediated by cracks, which have very complex load redistribution in the form of crack tip stress concentration, and the long range dipolar stress field. In order to remedy this deficiency, Arcangelis *et al.* introduced the random fuse model in 1985 [104] (Fig 1.4). This model can be thought of as a discrete coarse grained model of a disordered elastic material. In the random fuse model each fuse represents a material domain with a certain strength. The fuse can burn (just as the mate-

rial domain can break or fracture) when the current through it exceeds a certain threshold, at which point it becomes insulating and does not carry any more current. Thus, current is analogous to stress, where a material domain ruptures when the stress that it carries exceeds a threshold value, beyond which it cannot support any further stress. Such a model was discussed in spirit in some previous works [105, 106], however, it could be realized only after the advent of fast computers. It can be shown analytically that in a certain limit the two dimensional version of this model maps on to the anti-plane shear problem of fracture. Various variants of this model can be created by introducing different kinds of disorder. The most studied version of this model is based on percolation type disorder, where in each realization of the network, a fraction of bonds are removed with probability p. As the current is ramped up, fuses burn until there is no longer a conducting path in the network and it cannot support any further current (stress). At this point the network is said to be fractured. In a series of papers starting in 1986, Duxbury and co-workers have analyzed this model and solved it in the limit of small disorder [107–111]. They derived a distribution of failure strength based on nucleation theory which is sometimes called the Duxbury distribution. Kahng *et al.* studied a slightly different model in which fuses were not removed at random, rather they were given a random strength threshold taken from a known distribution [112]. In their model they used a uniform distribution with a gap at the origin. In this model they were able to observe a transition that was reminiscent of the brittle-ductile transition; however this analogy should be interpreted carefully as there are no plasticity or dislocation mechanisms in fuse network models. Similar effects were observed by Curtin [113, 114].

One aspect of fracture that is almost completely divorced from the contin-

uum description is that of avalanches and criticality. Experimental studies in fracture of diverse materials such as paper, glass, rocks and wood clearly suggest the existence of avalanches and critical fluctuations [115–120]. Both the statistical models of fracture, the fiber bundle [103, 121–130], and the fuse network capture this effect [131–144, 144–146]. Hansen and Hemmer solved the avalanche size distribution for the democratic fiber bundle exactly and found that the size distribution is a power law $P(s) \sim s^{-\tau}$, where τ is a universal critical exponent [121]. They found $\tau = 2.5$ for the integrated size distribution if avalanches within larger avalanches were not counted individually, and $\tau = 2.0$ otherwise. This result indicated that the democratic fiber bundle is in the mean field universality class, as one would expect. Zapperi *et al.* studied the avalanche size distribution in disordered fuse network and found an exponent close to the mean field value of 2.5 [136]. They also noticed that after considerable diffuse damage and avalanches, the fuse network broke in a giant avalanche, an event that resembled the nucleation and growth of an unstable crack. They interpreted this as a spinodal mode. Hansen and co-workers show that in the limit of infinite disorder, the fuse network problems maps to loopless percolation. They used this connection to argue that the universal crack roughness is due to percolation effects [9]. However, the idea that critical fluctuations which are characteristic of continuous phase transitions, can lead to fracture which is thought of as an abrupt transition, is strange. Sornette and co-workers have studied this problem in detail, and concluded that in a wide class of problems fracture is a true critical point [147–149], their functional renormalization group based analysis of another model of fracture is also worth noting [150].

Historically, the distribution of fracture strengths are studied under Weibull theory [151–174]. In a landmark paper in 1939 Weibull proposed a distribu-

tion for fracture strengths that fit a variety of data to remarkable accuracy [151]. Weibull's basic argument was that of the weakest link hypothesis. This hypothesis states that a large object is made up of several independent sub-volumes, and it breaks as soon as its weakest constituent breaks. This leads to the mathematical structure of statistics of extremes. Fisher and Tippett started the study of distribution of extremes in their landmark paper in 1928 [175]. The work of Fisher, Tippett and several other authors culminated in the 1943 paper by Gnedenko that established the mathematical foundations of extreme value statistics [176]. His work proved that in the limit of large samples, the distribution of extremes can take only three forms[1], the Weibull distribution being one of them. This subject was further developed in the works of several authors, the most prominent of them being E. J. Gumbel [152, 177–179, 179, 180].

There are three important questions that bring the use of Weibull theory into question. First, the mathematics of extreme provides for three limit forms, namely, the Weibull distribution, the Gumbel distribution, and the Fréchet distribution. Of these, the Fréchet distribution is not of relevance to fracture. However, there is no fundamental reason that prevents the Gumbel distribution to be the suitable limit distribution for fracture. In his analysis Weibull assumed a power law dependence of fracture probability on the applied stress, and thus he did not get a Gumbel distribution as the limit form; however, this assumption is questionable. Second, it is well known that the convergence to extreme value forms can be arbitrarily slow [3, 175, 181–183]. Given this slow convergence is it suitable to use the limit form for analyzing small data sets? And third, the mathematical structure of extreme values assumes uncorrelated variables, while in

[1] In extreme value theory the limit distributions are found under affine transformations of the arguments, and even so the limit does not always exist. See appendix A.1 for some details.

reality the fracture strengths of various regions in a material can be correlated. Does this effect the convergence or the rate of convergence to the limit forms? This thesis attempts to tackle some of these questions. It is worth mentioning that some recent developments have provided us with a fresh new way of looking at the classical extreme value statistics. In particular, the work of Györgyi *et al.* has developed a renormalization group based interpretation for extreme value statistics [184, 185], and the work of Bertin and Clusel has formulated the extreme value problem as a sum of correlated random variables [186]. I think that the mapping to the correlated sum has the potential to provide insights into the behavior of extremes of correlated random variables.

1.2 Arrangement of this Thesis

This thesis is primarily concerned with statistical models of fracture. The disordered fuse network is the primary model that is studied here. The ongoing work presented in appendix A.4 is the only place where I deal with continuum theories and atomistic models of fracture. There are two questions that are at the heart of this thesis. First is regarding the asymptotic distribution of fracture strength. Is the use of Weibull theory justified? Is the convergence to the extreme value forms rapid enough to justify their widespread use? Can we do better than using the Weibull distribution? Second concerns the understanding of fracture as a phase transition. How do we reconcile the fact that there are scale free distribution of avalanches and damage cluster in fracture, which is otherwise thought of as an abrupt first order transition? How do we understand the role of disorder in fracture? Another important question, though not addressed in this thesis, is that if one has to use the Weibull distribution to model fracture

strengths, then what is the optimal way of estimating the parameters?

Chapter 2 of the thesis addresses some issues of fracture strength distributions including their asymptotic properties and convergence rates. Chapter 3 presents our work on dielectric breakdown. Even though dielectric breakdown is not the same as fracture, it is closely related. We tackle several issues in this chapter that form a basis for our treatment of fracture in a later chapter. In particular, this chapter is a good buildup to our use of scaling functions and our treatment of critical points in the chapter concerning fracture. Chapter 4 sheds some light on the nature of the phase transition and critical properties associated with fracture. In this chapter we present a unified theory that uses renormalization group ideas to show how fracture can have properties of both abrupt and continuous phase transitions. We also introduce the novel concept of *finite-sized criticality* in this chapter. The appendices provides an introduction to the some of the mathematical tools that are central to understanding the content of this thesis. They also presents ongoing work on crack propagation that is not mature enough to merit a chapter yet. Appendix A.1 presents the basic results of extreme value statistics. Appendix A.2 discusses the basic theory of linear elastic fracture mechanics, while appendix A.3 presents a minimal discussion of Griffith's theory of fracture. Finally, appendix A.4 presents our work on crack paths in graphene.

CHAPTER 2

STRENGTH OF DISORDERED BRITTLE MATERIALS

2.1 Abstract[1]

We study the asymptotic properties of fracture strength distributions of disordered elastic media by a combination of renormalization group, extreme value theory, and numerical simulation. We investigate the validity of the 'weakest-link hypothesis' in the presence of realistic long-ranged interactions in the random fuse model. Numerical simulations indicate that the fracture strength is well described by the Duxbury-Leath-Beale (DLB) distribution which is shown to flow asymptotically to the Gumbel distribution. We explore the relation between the extreme value distributions and the DLB type asymptotic distributions, and show that the universal extreme value forms may not be appropriate to describe the non-universal low-strength tail.

2.2 Introduction

It has been known for centuries that larger bodies have lower fracture strength. The traditional explanation of this size effect is the 'weakest link' hypothesis: the sample is envisaged as a set of non-interacting sub-volumes with different failure thresholds, and its strength is determined by the failure of the weakest region. If the sub-volume threshold distribution has a power law tail near zero

[1]This chapter is published as Phys. Rev. Lett. 108, 065504 (2012) with co-authors C. Manzato, P. K. V. V. Nukala, M. J. Alava, J. P. Sethna, and S. Zapperi. I focussed on sections 2.3 and 2.5, and developed the software that was used for the simulations with minor modifications.

then the strength distribution can be shown to converge to the universal Weibull distribution for large sample sizes [151], an early application of extreme value theory (EVT) [179].

Often failure occurs due to the presence and growth of micro-cracks whose long-range interactions call the notion of independent sub-volumes into question. There have been two broad approaches to address such interactions: fiber bundle models and fracture network models [187]. Fiber bundles transfer load by various rules as individual fibers fail; in some particular cases exact asymptotic results for the failure distribution have been derived [188], and do not explicitly fall into any of the extreme value statistics universal forms. Fracture network models consider networks of elastic elements with realistic long-range interactions and disorder. A particularly simple approach is based on the random fuse model (RFM) [104,187], where one approximates continuum elasticity with a discretized scalar representation. It has been suggested that in the weak disorder limit, fracture would be ruled by the longest micro-crack present in the system [105,108,135,189]. This argument yields results that are accurate up to a prefactor; Phoenix and Beyerlein have given an exact calculation that computes the prefactor for the case of fiber bundles [188]. By using critical droplet theory type arguments, one can show that an exponential distribution of micro-cracks leads to the DLB distribution of failure strengths (up to a prefactor) [108], which again does not explicitly have an extreme value form.

These studies raise three important questions. First, what is the importance of elastic interactions in determining the strength distributions, and does the weakest link hypothesis hold in presence of such interactions? Second, what is the relation between the DLB type asymptotic strength distributions and the

universal forms predicted by EVT? Third, how should one best extrapolate from measured strength distributions to predict the probability of rare catastrophic events? We use renormalization group (RG) ideas, EVT, and simulations of the two dimensional RFM to explore these questions. We conclude that (i) the weakest link hypothesis is valid for large samples even in the presence of long-ranged elastic interactions, (ii) the asymptotic forms of the strength distribution for these interacting models is compatible in disguise with EVT, but of the Gumbel form rather than the Weibull form, and, (iii) the use of extreme value distributions to estimate the probability of rare events, though common in the experimental literature, is not always justified theoretically. DLB type asymptotic distributions (or those derived by Phoenix and Beyerlein [188]) which depend on the details of the material are necessary to safely extrapolate deep into the tails of the failure distribution.

2.3 Asymptotic Distributions of Fracture Strengths

The RG and the EVT present two equivalent, yet contrasting, approaches to the study of the universal aspects of extreme value distributions in general [185], and fracture strengths in particular. The natural framework to investigate the role of interactions and the corrections to scaling that emerge as the system size is changed is provided by the RG theory. In contrast, the EVT facilitates the study of domains of attraction and convergence issues. The non-universal, yet important, behavior of the low reliability tail of the distribution is not described adequately by either the RG or the EVT. To study such non-universal features one needs to develop DLB type asymptotic theories.

Typically, a RG transformation proceeds in two steps: in the first step the system is coarse-grained by eliminating short length-scale degrees of freedom, and then the resulting system is rescaled. The RG coarse-graining for fracture is equivalent to the weakest link hypothesis: a system of size L in $d = 2$ dimensions survives at a stress σ if its 4 ($= 2^d$) sub-systems of size $L/2$ survive at the same stress. This coarse-graining leads to the following recursion relation for $S_L(\sigma)$ — the probability that a system of size L does not fail under a stress σ:

$$S_L(\sigma) = [S_{L/2}(\sigma)]^4 . \tag{2.1}$$

The second step of the RG transformation is to re-scale the stress suitably and look for a fixed point distribution S^* that is invariant under RG

$$S^*(\sigma) = \mathcal{R}[S^*(\sigma)] = [S^*(a\sigma + b)]^4 . \tag{2.2}$$

Instead of applying Eq. 2.1 iteratively like the RG, the EVT formulation consider the large length-scale limit directly

$$S^*(\sigma) = \lim_{L\to\infty} [S_{L_0}(A_L\sigma + B_L)]^{(L/L_0)^d}, \tag{2.3}$$

where L_0 is a characteristic length-scale.

The functional equations 2.2, 2.3 are known to have only three solutions: the Gumbel, the Weibull, and the Fréchet distributions. Of these, only the Gumbel

$$S^*(\sigma) = \Lambda(\sigma) \equiv \exp[-e^{\sigma}],\ \sigma \in \Re,\ a = 1,\ b = \log 4, \tag{2.4}$$

and the Weibull

$$S^*(\sigma) = \Psi_\alpha(\sigma) \equiv e^{-\sigma^\alpha},\ \sigma, \alpha > 0,\ a = 4^{(-1/\alpha)},\ b = 0, \tag{2.5}$$

distributions are relevant for fracture. The large length norming constants, $A_L,\ B_L$, satisfy the following asymptotic relations $A_{2L}/A_L \to 1/a$, $|B_{2L} - B_L|/A_L \to$

b/a. As discussed in appendix A.1, given the microscopic distribution $S_{L_0}(\sigma)$, the fixed point of defined by Eq. 2.3, if it exists, is unique; and it is of one of the three forms discussed earlier. Details about the choice of the norming constants A_L, B_L can change the approach to the fixed point, but not the fixed point itself. Roughly speaking, the Weibull fixed point is approached if the tail of $S_{L_0}(\sigma)$ decays as a power law at a finite "left end"[2] of $S_{L_0}(\sigma)$, the Fréchet distribution is approached if the tail decays as a power law but the left end is not finite, and finally the Gumbel distribution is approached if the tail decays faster than any power law at either a finite or an infinite left end.

2.4 Numerical Validation

To test the validity of the weakest link hypothesis (Eq. 2.1) in presence of long-range elastic interactions, we perform large scale simulations of the RFM [104, 187], considering a tilted square lattice (diamond lattice) with $L \times L$ bonds of unit conductance. Initially we remove a fraction $1 - p$ of the fuses at random, where p is varied between $1 - p = 0.05$ and $1 - p = 0.35$ (the percolation threshold for this model is at $p = 1/2$). Periodic boundary conditions are imposed in the horizontal direction and a constant voltage difference, V, is applied between the top and the bottom of lattice system bus bars. The Kirchhoff equations are solved to determine the current distribution on the lattice. A fuse breaks irreversibly whenever the local current exceed a threshold that we set to one. Each time a fuse is broken, we re-calculate the currents in the lattice and find the next fuse to break. The process is repeated until the system is disconnected. In the present simulations, we have considered system sizes from $L = 16$ to $L = 1024$

[2]The "left end" of the distribution is defined as the largest σ such that $S_{L_0}(\sigma) = 1$

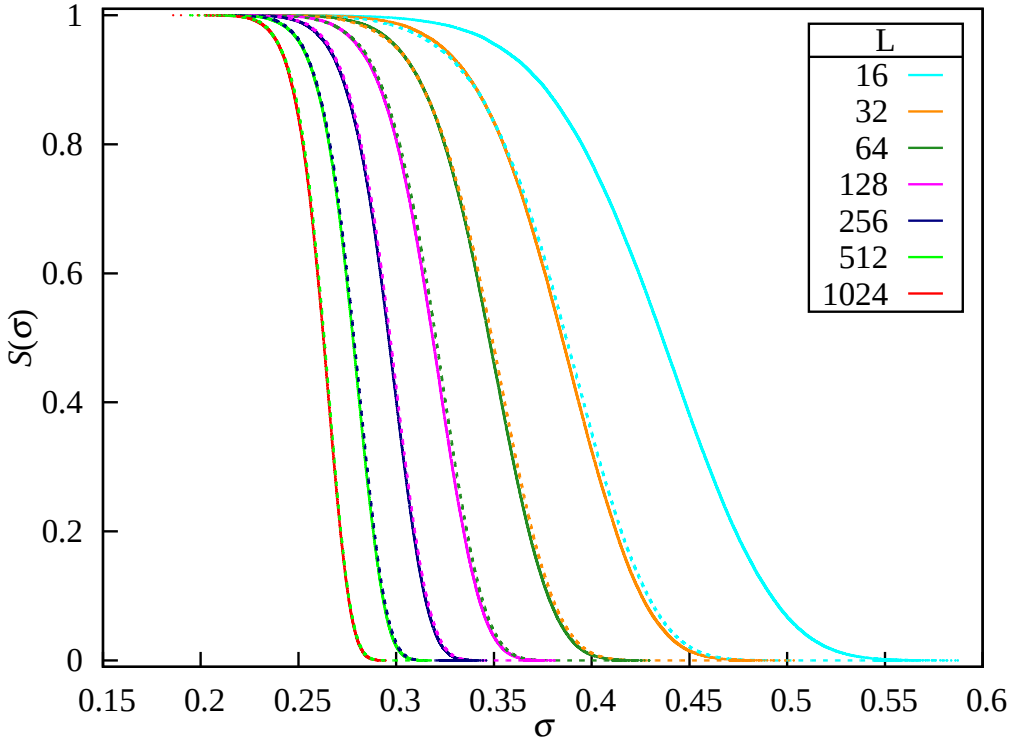

Figure 2.1: Testing the weakest link hypothesis. Comparing the survival probability $S_L(\sigma)$ for a $L \times L$ network (solid lines) with that predicted by the weakest link hypothesis, $S_{L/2}(\sigma)^4$, (dotted lines) for $1 - p = 0.10$. Note the excellent agreement even for moderate system sizes.

and various values of p. To explore the low strength tail which is beyond the accessible range of most experiments, we typically average our results over 10^5 realizations of the initial disorder. The fuse model is equivalent to a scalar elastic problem. Using this equivalence, the strain is defined as $\epsilon = V/L$ and the stress is given by $\sigma = I/L$, where I is the current flowing in the lattice. The fracture strength is defined as the maximum value of σ during the simulation.

The RG coarse-graining step (Eq. 2.1) produces a natural test for the weakest link hypothesis. In Fig. 2.1 we report the survival probability $S_L(\sigma)$ for different system sizes L, compared with those for systems of size $L/2$, rescaled according to Eq. 2.1. The agreement between the two distributions is almost perfect for

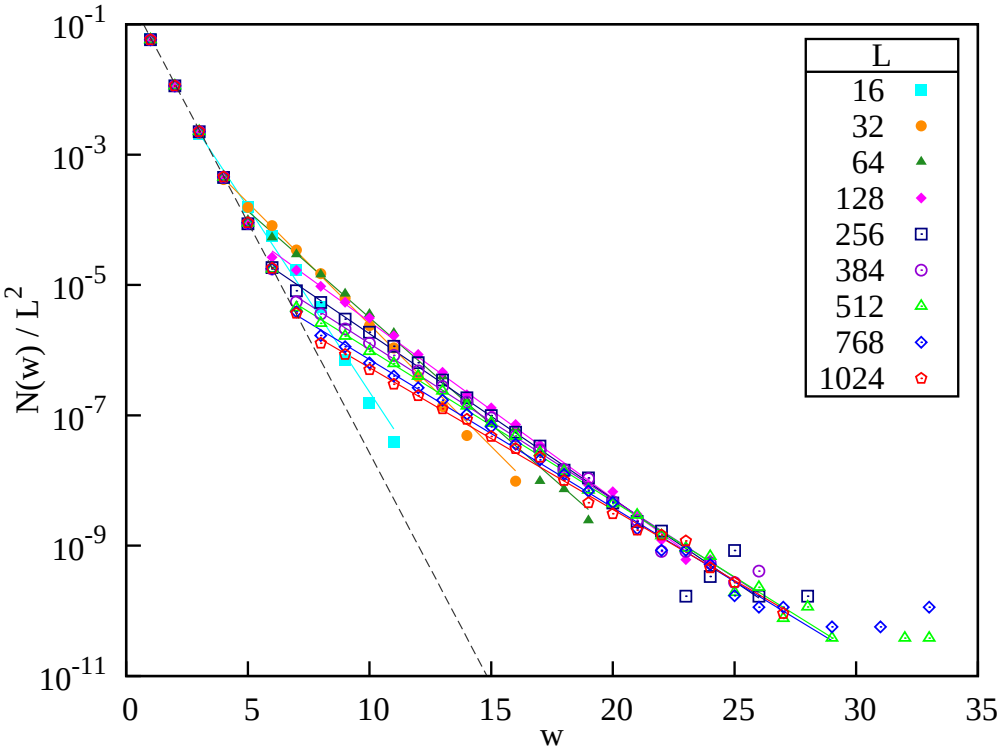

Figure 2.2: Crack width distributions at peak load with $1 - p = 0.10$. The initial distribution of micro-crack widths ($N(w)$ is the number of clusters of width w), is exponential with (dotted line, slope $\approx -\log 2(1-p)$). As the system is loaded, a few bonds break before catastrophic failure; these bonds usually connect smaller clusters, producing extra cracks at large widths. The resulting crack width distribution at the peak load exhibits a size-dependent crossover to a different exponential slope. Solid lines represent fits to an exponential.

$L/2 \geq 32$, indicating that Eq. 2.1 is satisfied asymptotically. Corrections to scaling due to the effect of distant micro-cracks are expected to decay as $1/L^2$, as can be shown by a direct calculation, but are too small for us to detect in simulations (Fig. 2.1). We also tested wide rectangular systems with $L_x = 2L_y$, finding larger corrections, scaling roughly as $1/L$, which are still irrelevant in the large system size limit.

Duxbury *et al.* related the survival distribution to the distribution of micro-crack widths w [108]. At the beginning of the simulation the 'per-site' prob-

ability distribution of a crack of width w is $P(w < w') = 1 - e^{-w'/w_0}$, where $w_0 \sim -1/\log 2(1-p)$. The factor 2 in $w_0 \sim -1/\log 2(1-p)$ is due to the fact that, on the diamond lattice, there are 2^w crack 'backbones' of width w with a given site as their left end. Hence, the distribution of the longest crack, w_m, in a lattice with L^2 sites is given by

$$P(w_m < w') = \left(1 - e^{-w'/w_0}\right)^{L^2}. \tag{2.6}$$

The stress at the tip of a crack of width w is asymptotic to $\sigma K\sqrt{w}$, where σ is the applied far-field stress, and K is a lattice dependent constant. A sample survives until the largest crack becomes unstable when its tip stress reaches a threshold $\sigma_{th} = \sigma K\sqrt{w}$. Therefore, we have

$$S_L(\sigma) \simeq \left(1 - e^{-(\frac{\sigma_0}{\sigma})^2}\right)^{L^2} \simeq D_L(\sigma), \tag{2.7}$$

where $\sigma_0 \equiv \sigma_{th}/K\sqrt{w_0}$ and $D_L(\sigma) \equiv \exp[-L^2 e^{-(\sigma_0/\sigma)^2}]$ is the DLB distribution. To apply the above derivation to the failure stress, we first check the distribution of micro-crack lengths at peak load. As shown in Fig. 2.2, the distribution is exponential, but due to damage accumulation, the slope of the tail changes with respect to the initial distribution. This appears to be due to bridging events in which two neighboring cracks join, leading to a modification of Eq. 2.7 as discussed in Ref. [108]. Thus, damage accumulation, though very small, is relevant because it changes the exponent of the micro-crack distribution. The exponential form of the crack length distribution tail, however, suggests that the DLB form should still be valid, as demonstrated in Fig. 2.3. In particular, the average failure stress scales as $\langle\sigma\rangle = \sigma_0/\sqrt{\log(L^2)}$ (Fig. 2.3) and the distributions for different L all collapse into a straight line when plotted in terms of rescaled coordinates (Fig. 2.4).

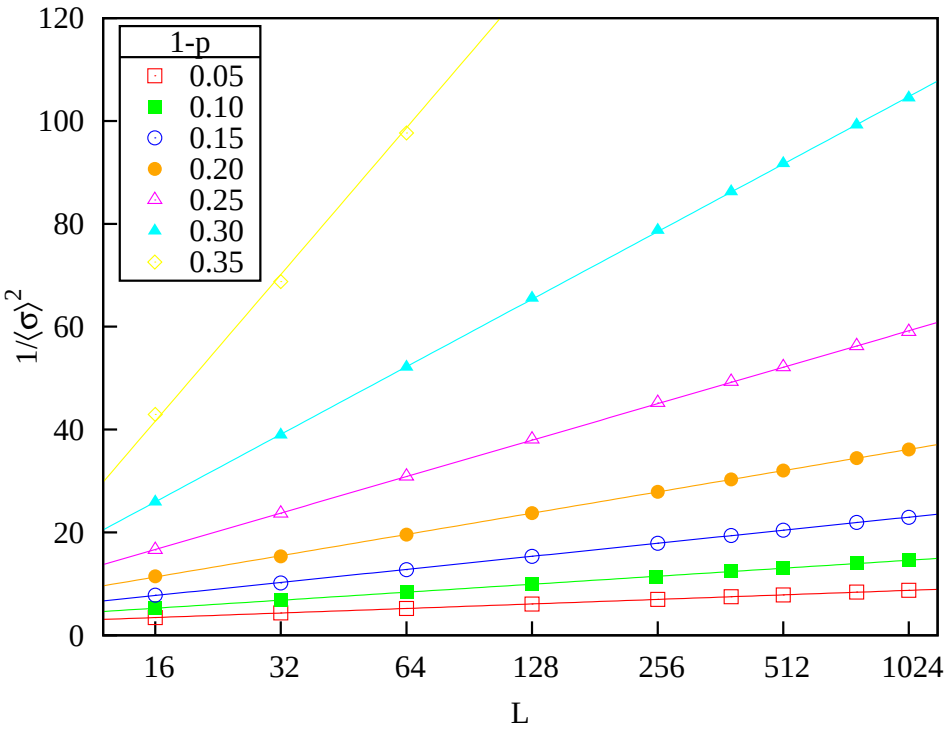

Figure 2.3: The average failure stress as a function of system size L at various bond fractions p (symbols) can be fit well by the DLB form (solid lines), except close to the percolation threshold ($1 - p > 0.3$).

2.5 Convergence and Asymptotic Properties

Our arguments thus far are seemingly paradoxical. On the one hand we have argued on very general grounds that the distribution of failure strengths must be either Gumbel or Weibull, while on the other hand we have checked that the failure distribution for fuse-networks is of the rather different form proposed by Duxbury *et al.* How can this 'paradox' be resolved? While it is not guaranteed that a microscopic survival distribution will lead to a fixed point under linear rescaling (Eqs. 2.2, 2.3), the DLB distribution does converge to the Gumbel form, i.e.,

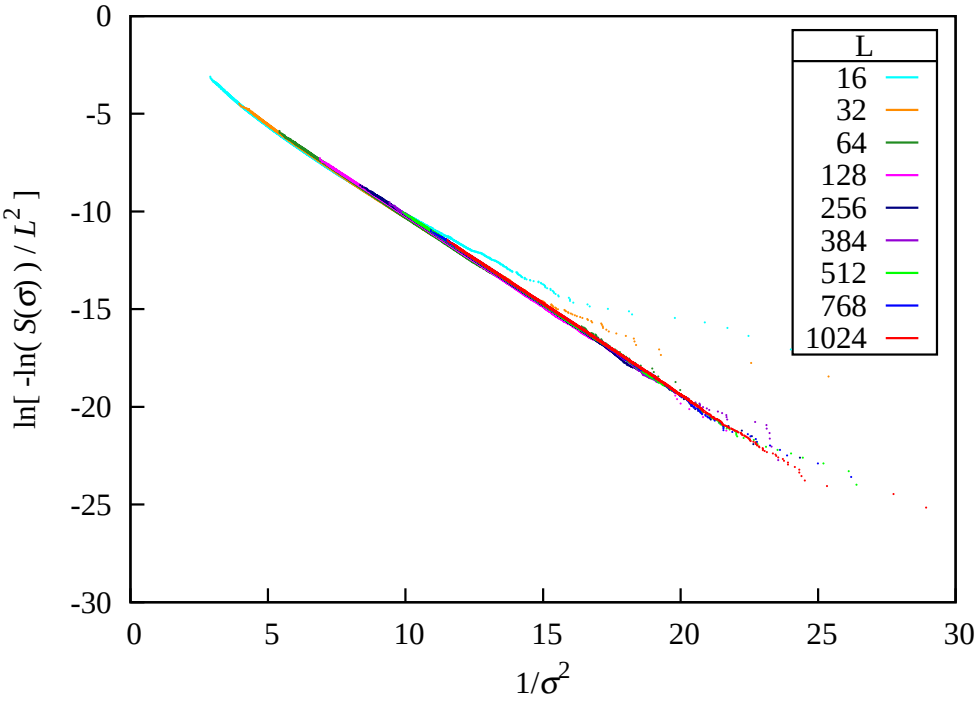

Figure 2.4: A collapse of the strength distribution for different system sizes at $1 - p = 0.1$, such that the DLB form would collapse onto a straight line.

$$\lim_{L\to\infty} D_L(A_L\sigma + B_L) = \Lambda(\sigma), \tag{2.8}$$

as can be demonstrated by a straightforward calculation using $A_L = \sigma_0/(2(\log(L^2))^{3/2})$ and $B_L = \sigma_0/\sqrt{\log(L^2)}$. The above result is striking because fracture distributions are usually assumed to not be of the Gumbel form, since fracture must happen at positive stress, while the Gumbel distribution has support for negative arguments as well. This is akin to arguing that the normal distribution is not valid for test scores since scores must always be positive. Nonetheless, it brings us to the issue of convergence and validity of extreme value distributions as opposed to DLB type distributions.

The extreme value distributions, $S^*(\sigma)$ (=$\Lambda(\sigma)$ or $\Psi_\alpha(\sigma)$), are a uniform approximation to the true survival function, $S_L(\sigma)$, for all σ in the limit of large L, i.e.,

$$\lim_{L\to\infty}\left(\sup_{\sigma\in\Re}\left|S_L(\sigma)-S^*\left(\frac{\sigma-B_L}{A_L}\right)\right|\right)=0. \tag{2.9}$$

In contrast, DLB type distributions [3], are based on material details, and are asymptotically correct in the low reliability tail, i.e.,

$$\lim_{L\to\infty}\left(\lim_{\sigma\to 0}\frac{1-D_L(\sigma)}{1-S_L(\sigma)}\right)=1. \tag{2.10}$$

Note that the uniform convergence in Eq. 2.9 does not bound the *relative* error in the low reliability tail, while the asymptotic convergence in Eq. 2.10 does.

The above discussion hints at an underlying question: How to accurately predict the probability of rare small-strength events with limited experimental data? The standard practice is to measure the failure distribution of construction beams or micro-circuit wires, fit to the universal Weibull or Gumbel form, and extrapolate. However, as we have argued, this approach can lead to incorrect estimates. The low reliability tail is non-universal, and must be modeled by a theory that, like DLB, accounts for microscopic details (see also [190]). Such theories, analogous to critical droplet theory (low temperatures), instantons (low $\hbar$), and Lifshitz tails (low disorder, deep in the band gap) are by construction accurate in the low reliability tail. In this case a fit to the Weibull or Gumbel form over-estimates the low-stress failure probability, and hence might be appropriate as a conservative estimate (e.g., construction beams), but not when optimizing a design (e.g., circuits). It is interesting to observe that usually the RG and the critical droplet theory address continuous and abrupt phase transitions, respectively, yet here these two approaches both apply to fracture.

[3] The DLB distribution is asymptotically exact (up to a prefactor) in the limit of $1-p\to 0$

The convergence to extreme value distributions can be extremely slow [190]. For the RFM, let z be number of standard deviations up to which the Gumbel approximation is accurate within a relative error of ϵ. By using the Edgeworth type expansions for the extreme value distributions [183], we find

$$\frac{z\pi}{\sqrt{6}} = \begin{cases} \sqrt{\eta}\exp[-\frac{\sqrt{\eta}}{2}\exp[-\frac{\sqrt{\eta}}{2}\exp[\ldots]]], & \eta < 4e^2 \\ \log\eta - 2\log[\log\eta - 2\log[\ldots]], & \eta > 4e^2, \end{cases}$$

where the ellipsis indicate an infinite recursion, and $\eta = -(4/3)\log(1-\epsilon)\log(L^2)$. For an accuracy of 10% at one standard deviation a sample volume of $L^2 \approx 10^{18}$ is required, while at 2 standard deviations the required sample volume is about $L^2 \approx 10^{264}$. As a comparison, for the Gaussian approximation to the mean of a sample of $M(\gg 1)$ random variables (normalized so that $E[X] = 0$, $E[X^2] = 1$, $E[X^3] = \gamma$) we get, $z \sim \Delta^{1/3} + \Delta^{-1/3} + O(\Delta^{-4/3})$, where $\Delta = 6\epsilon\sqrt{M}/\gamma$, thus $z \approx 3$ for $\epsilon = 0.1$, $M = 3000$, $\gamma = 2$, where the value $\gamma = 2$ corresponds to the standard exponential distribution. However, the universal extreme value forms are not always dangerous for extrapolation. One can show that they are valid asymptotic forms, à la Eq. 2.10, if they satisfy the condition of tail equivalence [3, p. 102] [182]:

$$\lim_{\sigma\to 0}\frac{1-S_L(\sigma)}{1-S^*(\sigma)} = C,\ 0 < C < \infty. \tag{2.11}$$

The success of the classical example of a Weibull distribution of failure strengths emerging from a power-law micro-crack length distribution may be due to the tail equivalence of the microscopic and the Weibull distributions.

2.6 Conclusion

In conclusion, by using a combination of renormalization group, extreme value theory, and numerical simulations we have shown that the failure strength of an elastic solid with a random distribution of micro-cracks follows the DLB distribution which asymptotically falls into the Gumbel universality class. The non-universal low reliability tail of the strength distribution may not be described by the universal extreme value distributions, and thus the common practice of fitting experimental data to universal forms and extrapolating in the tails is questionable. Theories that account for microscopic mechanisms of failures [190], the DLB distribution for instance, are required for accurate prediction of low strength failures. In our study the emergence of a Gumbel distribution of fracture strengths is surprising, and brings into question the widespread use of the Weibull distribution for fitting experimental data.

CHAPTER 3

AVALANCHES AND DIELECTRIC BREAKDOWN

3.1 Abstract[1]

Motivated by recent experiments on the finite temperature Mott transition in VO_2 films, we propose a classical coarse-grained dielectric breakdown model where each degree of freedom represents a nanograin which transitions from insulator to metal with increasing temperature and voltage at random thresholds due to quenched disorder. We describe the properties of the resulting non-equilibrium metal-insulator transition and explain the universal characteristics of the resistance jump distribution. We predict that by tuning voltage, another critical point is approached, which separates a phase of boltlike avalanches from percolationlike ones.

3.2 Introduction

Vanadium dioxide (VO_2), when heated or strained, displays an insulator to metal transition with intriguing non-equilibrium collective behavior, portrayed in a remarkable series of recent experiments [191–195]. Strong electron correlations drive the microscopics of this metal-insulator transition, where a delicate interplay among structural, electronic and spin degrees of freedom takes place [196]. However, as we argue in this Letter, the universal features of the observed resistance jumps can be understood via appropriate generalizations

[1]This chapter is published as Phys. Rev. Lett. 107, 276401 (2011) with minor modifications. The co-authors are S. Papanikolaou, S. Zapperi and J. P. Sethna.

of previously studied models of dielectric breakdown [107,197]. By tuning two natural control parameters, the applied voltage V and the contrast h (the ratio of conductances of the insulating and metallic domains), we show that the existing experiments are in the small h regime, where a crossover, in small samples, between a low-V percolating phase and a high-V "bolt" phase takes place. As h becomes larger, this crossover evolves to a sharp transition with novel critical properties.

The VO_2 films studied in Ref. [191] had a thickness of 90 nm, widths ranging from 2 μm to 15 μm and lengths ranging from 200 nm to 4 μm. X-ray diffraction studies of films near criticality revealed that stable insulating grains have an average linear size of 20 nm [192,198]. With the sample put under an external voltage V, multiple resistance jumps were observed near the bulk transition temperature [191]. Let ΔR be the resistance change that occurs during one such jump. The statistics of these jumps revealed a power law probability distribution $P(\Delta R) \sim \Delta R^{-\alpha}$, with an exponent $\alpha \simeq 2.45$. The resistance jump distribution depended strongly on the magnitude of the external voltage, with the largest jump scaling linearly with the voltage. Further, in the presence of external voltage, elongated conducting clusters have been observed through X-ray diffraction [192], whereas in the absence of voltage, percolationlike isotropic clusters have been recorded with near-field infrared spectroscopy [193,199].

Even though VO_2's transition properties are dominated by electron correlations, we argue that the observed collective phenomena can be explained in a purely classical way, consistent with experimental observations [191–195]. The large length scales of the domains (~15-20 nm) and the small electron mean-free path near the transition (~0.26 nm) suggest that coherence effects are unimpor-

tant and electron transport is predominantly classical (Ohm 's law). Given the observed metallic domain sizes of 20 nm and the sample thickness of 90 nm, it is clear that avalanches involving domains at distances larger than 5 lattice spacings have a 2D character, thereby justifying the use of our 2D model. This high-temperature transition (~340 K) cannot be interpreted as a quantum phase transition, since the observed ~1% lattice distortion suppresses any electronic coherence. The Frank-Condon overlap integral, accounting for the ~1% lattice distortion, would drastically suppress any quantum overlap between electronic initial and final states on these length scales (~20 nm). The thermal loading must be considered quasi-static because the loading rate of the experiments (< 3 K/min, [191]) is much slower than the intrinsic dynamics of the domains (~10^{-3} s, [198]). Also, some experiments at high voltage show a large event that repeats in space [200] and time [194] over repeated cycles of thermal loading, while others [191], for smaller voltages do not exhibit this repetition. In our model, we consider a quasi-static model of classical resistors in two dimensions with deterministic dynamics, and with classical, quenched disorder, hence leading to reproducible avalanche sequences. The strongly-correlated quantum and statistical physics underlying the Mott transition is absorbed into temperature and voltage dependencies of our domain dynamics, which could be estimated by using DMFT methods [201, 202].

Motivated by previous successful studies of strongly-correlated electronic systems at finite temperatures [203–205], we propose an extended dielectric breakdown network model of coarse-grained regions transforming from insulator to conductor with random critical temperature thresholds. We study the resistance jump distribution and make predictions about the exponent α. In addition, we study the probability distribution of avalanche sizes $P(s) \sim s^{-\tau}$, where

s is the number of resistors transformed in a single avalanche burst. We explain the observed qualitative behavior at different voltages, and predict the existence of two distinct regimes: a) a percolation dominated regime [206] where scaling appears only in resistance jumps and avalanches are isotropic and small, and, b) a bolt dominated regime, where avalanches are highly anisotropic, almost linelike. Finally, we make a number of experimentally verifiable predictions regarding the behavior of the system in the different regimes.

3.3 Coarse Grained Model

In our model each link i of the network, labelled by a variable S_i, is thought of as a microscopic "grain" of linear size at least of the order of the dephasing length l_ϕ. It can be conducting ($S_i \equiv +1$) with conductance σ_C, or insulating ($S_i \equiv -1$) with conductance $\sigma_I = h\,\sigma_C$. The variable $0 \leq h \leq 1$ is the inverse contrast between conducting and insulating regions. We enforce bi-periodic boundary conditions on a diamond lattice (a square grid rotated by 45°) and subject it to an external voltage V per link. Experimental observations show that the threshold temperature in the insulator to metal transition decreases with voltage [195,200, 201]. We account for this in the model by transforming the resistor at link i from insulator to metal when the following condition is satisfied,

$$T \geq T_i^c - bV_i \tag{3.1}$$

where T is the temperature of the sample, V_i is the voltage drop across the i^{th} link, and T_i^c is the random zero-voltage critical temperature threshold which models the disorder. The unit of resistance is $\Delta R = (1-h)R_I$, for a single resistor. The quantity R_I is defined by the resistance deep in the insulating phase

(when all grains are insulating), and here we set it to unity. The unit of voltage and temperature in our simulation is the variance of the random pinning field disorder (assuming $b = 1$). Equation 3.1 is a linear approximation to the observed voltage dependence of the critical temperature threshold [195, 200, 201]; the exact functional form should be irrelevant for the universal behavior.

3.4 Analysis

In this model there are two cases which have been studied previously: $V = 0$ and the limit $h \to 1$. At $V = 0$, resistors are not coupled and transform sequentially one at a time as in percolation. The resistance jump distribution for percolation, originally studied in Ref. [206], displays a multifractal structure with a power law tail at large jumps decreasing with an exponent $\alpha \simeq 2.7$ (the power law tail is shown in Fig. 3.1(b)). As $h \to 1$, the model can be studied by an explicit perturbation expansion in powers of $(1 - h)/h$ [207]. The voltage V_i across the i^{th} link satisfies the recursive equation $V_i = V - \frac{1}{2}[(1 - h)/h] \sum_j \Gamma_{ij}(S_j + 1)V_j$, where Γ_{ij} are the lattice Green functions with dipolar form at long distances. Their general form for a n-dimensional hyper-cubic lattice is $\Gamma_{ij} = \int d^n k/(2\pi)^n \sin\frac{1}{2}k_i \sin\frac{1}{2}k_j \cos(\mathbf{k}.\mathbf{r}_{ij})/(\sum_{l=1}^{n} \sin^2\frac{1}{2}k_l)$, where k_i, k_j are the directional wave vector components, and $\mathbf{r}_{ij}$ is the vector from the center of link i to center of link j. Taking $\epsilon \equiv (1 - h)/h << 1$ we obtain [207],

$$V_i - V = -(\epsilon V/2)\Sigma_j \Gamma_{ij}(S_j + 1) + O(\epsilon^2). \tag{3.2}$$

Thus, in the singular limit of $h \to 1$, the model maps to a disordered, long-range, frustrated Ising model. This mapping is intriguing, because it maps a dielectric breakdown model with *non-additive* multi-body interactions, to a dipolar

Ising model with additive two-body interactions. The dipolar interaction in this singular limit is shared with a model [208] of interface depinning in magnetic hysteresis, where their fingerlike structures resemble our bolts.

3.5 Numerical Validation

We perform numerical simulations, where a random temperature threshold T_i^c, drawn from the standard Gaussian distribution, is assigned to each link. The simulation starts with every resistor in the insulating state ($S_i = -1 \; \forall \; i$). The voltage at individual nodes is found by numerically solving the Kirchoff equations [209]. At each step the resistor for which the condition $T = T_i^c - b|V_i|$ (Eq. 3.1) is satisfied at the lowest possible value of T, is transformed into metal, and voltages are recomputed for the entire network. The process is repeated until every resistor in the conducting state ($S_i = 1 \; \forall \; i$).

In the experiments of Refs. [191, 192, 199] on VO_2, h is small (about 10^{-3}) and the voltage appears to be low compared to the disorder threshold. In this limit, for large resistance jumps, shown in Fig. 3.1(a), the distribution has an exponent $\alpha \simeq 2.7$ which is very similar to the experimental findings reported in Ref. [191]. The structure of the resistance-temperature curve shown in Fig. 3.1(b) is also similar to ones reported experimentally. The size of the largest resistance jump scales linearly with the applied voltage, as reported in Ref. [191]. This dependence on the applied voltage stems from the non-additive multi-body interactions of our model, and cannot be achieved by previously suggested bond-percolation type models [191] where the size of the largest resistance jump vanishes in the large system size limit. A more explicit signature of percolation

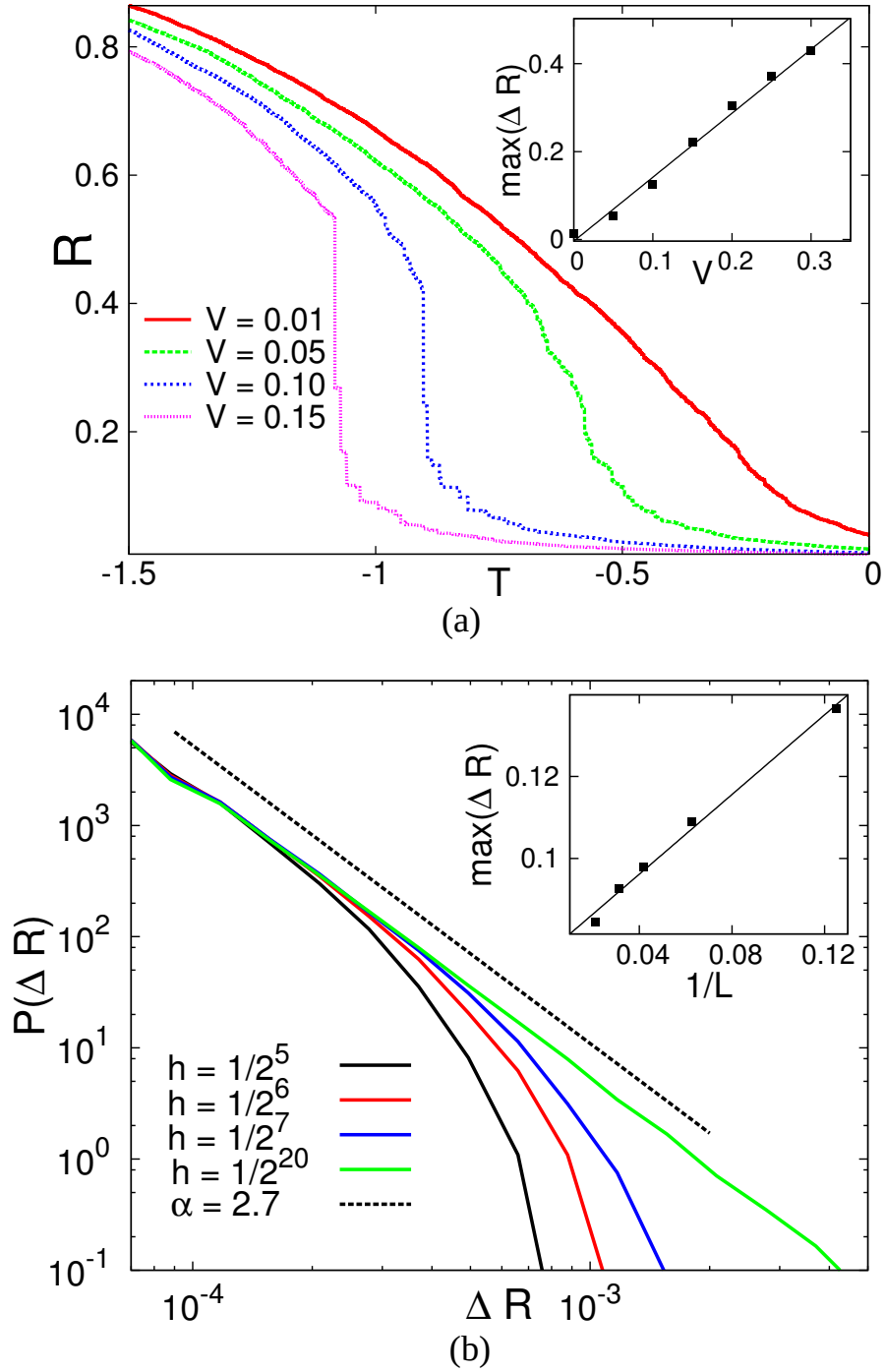

Figure 3.1: **Universal scaling and avalanches in the high-contrast, percolation-dominated regime**. (a) The resistance-temperature curve shows a multiple-step structure similar to the experimentally observed one [191]. (b) The resistance jump distribution acquires a universal form, for different contrast parameters and voltages for $L = 128$. The exponent $\alpha = 2.7$ agrees qualitatively with the experimentally observed exponent 2.45. Additionally, the distributions show finite-size scaling, demonstrating the presence of a nearby critical point. **Insets**: The largest resistance jump is observed to scale linearly with $1/L$ at fixed $V = 0.1$ (inset in (b), as observed experimentally [191]), and linearly with V at fixed $L = 128$ (inset in (a)) .

would be the observation of the multifractal scaling [206] expected at low resistance jumps, possibly below the experimental resolution.

3.6 Scaling Analysis and Phase Transition

When the contrast is smaller ($h \gtrsim 1/2$), we find that the insulator to metal transition occurs in avalanches, with several bonds transforming simultaneously at the same temperature. For fixed h (near 1), avalanches and resistance jumps are linearly related ($\Delta R \sim s(1-h)/(2L^2)$ for the diamond lattice) and both show power laws and universal scaling (sizes shown in Fig. 3.2). As the external voltage V is varied, the avalanche size distribution evolves from trivial (at $V = 0$, where resistors transform one by one) to a power law at a critical voltage $V_{\rm cr}(h)$, to again trivial (one giant avalanche) at $V \gg V_{\rm cr}$. This behavior is suggestive of a continuous phase transition; we analyze the probability distribution of our sizes $P(s)$ with the scaling form $P(s) \sim s^{-\tau}\Phi(s/\xi^{\sigma}, L/\xi)$, where $\xi \sim |V - V_{\rm cr}|^{-\nu}$ is the correlation length. The n^{th} moment of the avalanche size distribution scales as $\langle s^n \rangle \sim L^{\sigma(1+n-\tau)}\Psi((V - V_{\rm cr})L^{1/\nu})$. These scaling forms fit the data with good accuracy as shown in Fig. 3.2. Figure 3.2(a) shows the universal size distribution and Fig. 3.2(b) shows the distribution of the mean avalanche size, and a fit to the predicted scaling form. From these fits we get $1/\nu = 0.25 \pm 0.24$, $\sigma = 0.8 \pm 0.4$, $\tau = \alpha = 1 \pm 0.2$. We have also studied other disorder distributions (e.g. T_i^c taken from a uniform or exponential distribution) and explored other analytical methods (e.g. changing the critical range in the fits and analyzing the size distribution of spatially connected pieces of the avalanches) all of which confirm the presence of critical fluctuations.

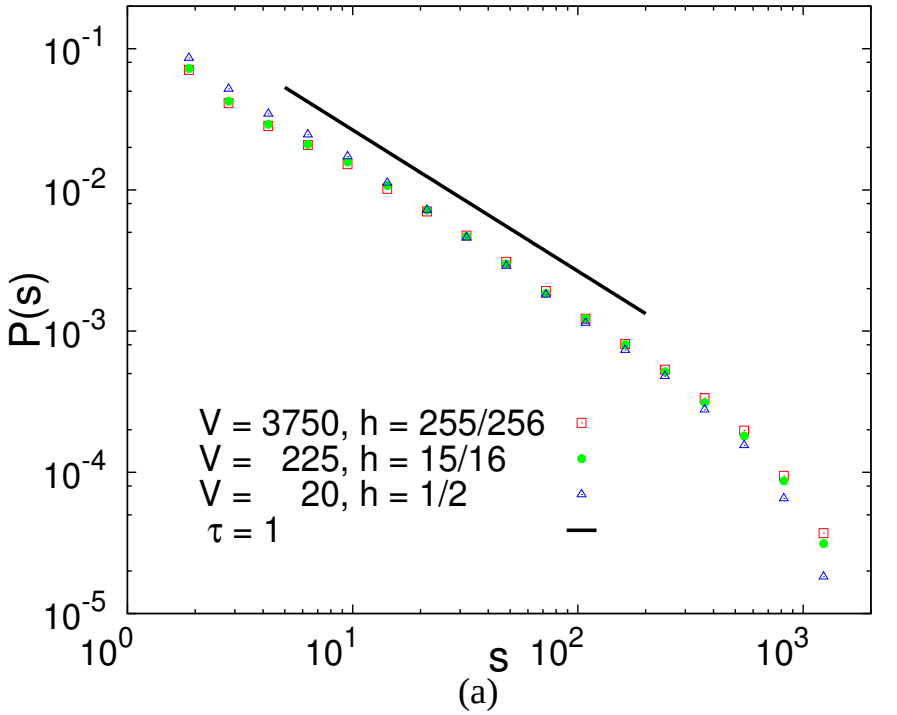

(a)

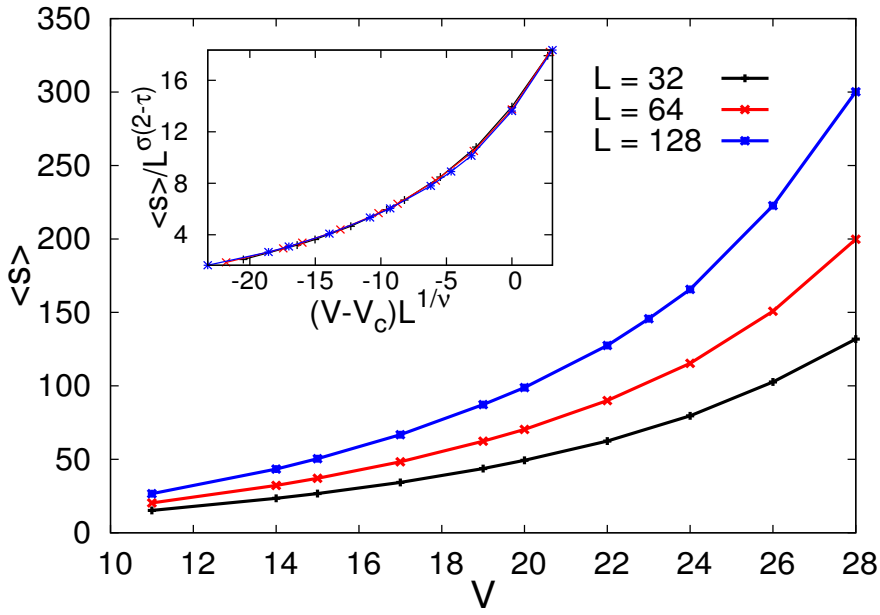

(b)

Figure 3.2: **Novel universality at the percolation-bolt transition.** (a) The probability distribution of avalanche sizes shows universal scaling near $h = 1$; In this limit, $\Delta R \sim S$. (b) As shown in the inset, the mean avalanche size at the critical voltage diverges as $L \to \infty$, suggesting a continuous phase transition.

The phase transition identified above separates a percolative phase from a 'bolt' phase as shown in Fig. 3.3. We estimate the phase boundary by a mean-field theory that becomes exact in the limit of $h \to 1,\ V \to 0$. In this limit the local voltage concentrations are unimportant and the interactions are additive. The avalanches can be modeled as a branching process – a grain (bond) turning metallic induces a long-ranged perturbation in the voltage field, which can result in a few more grains turning metallic, ad infinitum. The voltage change, ΔV, due to a single metallic bond at a distance r, goes as $\Delta V(r) \propto \frac{V(1-h)}{r^2(1+h)}$ (a continuum result obtained by approximating a single metallic bond by a circular inclusion in a 2-D domain). Let λ be the average number of grains that turn metallic due the perturbation caused by one grain, then $\lambda \propto V \log L(1-h)/(1+h)$. The mean size of the resulting avalanche is given by $1 + \lambda + \lambda^2 + \ldots$. Thus, setting $\lambda = 1$ yields a phase boundary between a phase with small avalanches (percolative phase, $\lambda < 1$), and a phase with large avalanches (bolt phase, $\lambda \geq 1$).

Figure 3.3 shows the phase boundary $V = 7.26(1+h)/(1-h)$, where the prefactor 7.26 is obtained by fitting the simulation data. It is difficult to notice the logarithmic drift in the phase boundary due to limited simulation size, however, the mean-field analysis suggests that the phase boundary is at $V = 0$ in the limit of $L \to \infty$. Even though the voltage per bond, V, goes to zero, the externally applied voltage diverges as $L/\log L$. This is analogous to fracture where the stress at failure goes to zero, and yet the net applied force at failure diverges in the limit of large length scales [187]. The mean-field theory yields an avalanche size exponent of $\tau = 3/2$, which is different from the numerically observed value (Fig. 3.2 a), possibly due to the effect of fluctuations. Finally, we have checked that the mean-field theory can also be collapsed by using scaling forms consistent with the scaling analysis discussed previously (Fig. 3.2 b).

Even though we believe that the phase diagram shown in Fig. 3.3 is qualitatively accurate, there are other possible scenarios that cannot be entirely ruled out. It is possible that V is finite at the transition, as suggested by the scaling analysis. It is also possible that this is an avoided critical point, *i.e.* large avalanches reflecting a crossover to the critical point at $h \to 1, V \to \infty$. However, the avalanche size distribution displays a scaling collapse (cf. Fig. 2) and a power law in a large range. Also, the behavior is fairly independent of h for $0.5 < h < 1$, rendering a crossover unlikely.

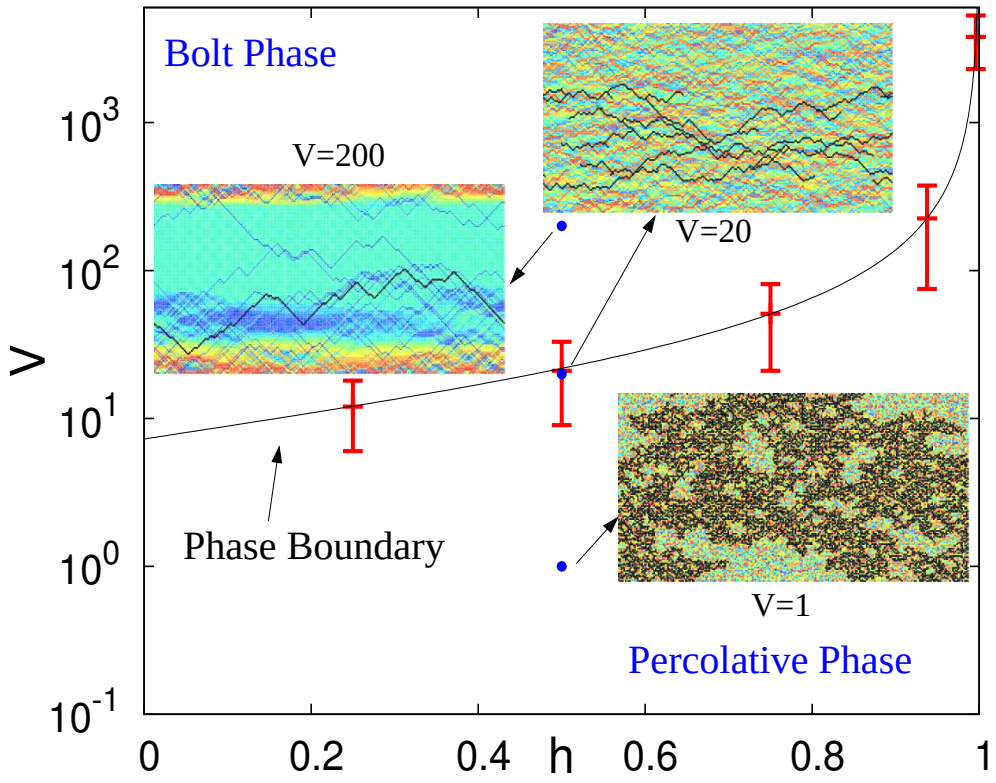

Figure 3.3: **Fractal-looking clusters and phase diagram**. The colors in the insets reflect avalanches; the first spanning cluster is shown in black. The phase boundary and the error-bars are obtained by treating the critical voltage, V_{cr}, as a free parameter in data collapses (see Fig. 3.2). The percolation fixed point at $h = 0, V = 0$ is likely unstable under coarse-graining, and we anticipate that there will be a crossover to the critical point ($h \to 1$) behavior for very large avalanches even for high contrast.

Our minimal model can be verified experimentally in the following ways: a) For high voltages boltlike avalanches should appear, leading to boltlike conducting clusters. This property has already been observed in Ref. [192], where elongated clusters appear in the presence of finite gate voltage, whereas such anisotropy is absent when $V = 0$ [199]. b) At low contrast ($h \gtrsim 1/2$), mean resistance jumps and sizes (measured, e.g., using multiple ESM images) should diverge only at a critical voltage, with power law distributions $\tau = \alpha \simeq 1$. An approach to this regime should be easier in hydrostatic pressure-controlled systems like organic materials in the κ-ET family.

3.7 Conclusions

In conclusion, we presented a novel model of avalanches for the metal-insulator transition in VO_2, bringing together recent experimental findings, and also making concrete experimental predictions as the relevant parameters are altered. We have identified a novel continuous transition controlled by long-range interactions which could be observed in particular classes of materials that have evidently smaller contrast, like organic materials under hydrostatic pressure [210,211] or bulk V_2O_3 [212]. Another possibility for achieving low contrast is by tuning hydrostatic pressure, approaching the metal-insulator Ising critical point [205].

CHAPTER 4

AVALANCHES IN FRACTURE

4.1 Abstract[1]

We present a unified theory of fracture in disordered brittle media that reconciles apparently conflicting results reported in the literature. Our renormalization group based approach yields a phase diagram in which the percolation fixed point, expected for infinite disorder, is unstable for finite disorder and flows to a zero-disorder nucleation-type fixed point. In a region of intermediate disorder and finite system sizes, we predict a crossover region with mean-field avalanche scaling. We discuss intriguing connections to other phenomena where critical scaling is only observed in finite size systems and disappears in the thermodynamic limit.

4.2 Introduction

Brittle fracture in disordered media intertwines two phenomena that seldom coexist, namely, nucleation and critical fluctuations. The usual dichotomy of thought between nucleated and continuous transitions makes the study of fracture interesting. Even more intriguing is the fact that crack nucleation happens at zero stress in the thermodynamic limit: smaller is stronger and larger is weaker. This makes the existence of critical fluctuation in form of clusters and avalanches of all sizes even more mysterious. What kind of critical

[1]This chapter is published as Phys. Rev. Lett. 110, 185505 (2013). The co-authors are S. Zapperi and J. P. Sethna.

point governs a phase transition that happens at zero applied field (stress) in the thermodynamic limit, and what is the universality class of such a transition? How do self-similar clusters, extremely rough crack surfaces, and scale invariant avalanches ultimately give rise to sharp cracks and localized growth? These questions have been addressed previously via a host of different theories, such as those based on percolation and multifractals [9, 213], spinodal modes and mean-field criticality [136], and classical nucleation [108]. In this Letter, we present a theoretical framework based on the renormalization group and crossover scaling that unifies the seemingly disparate descriptions of fracture into one consistent framework.

Fracture in disordered media is the result of a complex interplay between quenched heterogeneities and long-range stress fields leading to diffuse damage throughout the sample, and local stress concentration favoring the formation of sharp localized cracks. The self-affine morphology of cracks [214], the power law statistics of avalanche precursors [116, 117, 120, 121, 187, 215] and the scale dependence of the failure strength distribution [94, 95, 103, 112, 134, 187, 215–217] all result from this competition. Disordered fracture can be understood in the limit of infinitesimal as well as infinite disorder. Infinitesimal disorder means perfect crystalline material with just a few isolated defects (say a missing atom or a micro-crack). In this limit, fracture statistics can be understood as a nucleation type first order phase transition [107, 108, 135, 218]. In the limit of infinite disorder, stress concentration becomes irrelevant and fracture progresses via uncorrelated percolation-like damage [9, 213]. This mapping to percolation theory becomes rigorously valid when the disorder distribution is not normalizable (or *very broad*, in the language of multifractals) [213]. The situation is more complicated at intermediate disorder, where unlike typical first order transi-

tions, crack nucleation is preceded by avalanches with power-law distributions and mean-field exponents [121, 136, 144, 146, 215], sometimes interpreted as a signature of a spinodal point [136]. Our renormalization group based theory unifies the above descriptions into one consistent framework that is summarized into a single phase diagram.

4.3 Fuse Network Model

We use a 2D fuse network to model disordered brittle materials. A description of the disordered fuse network model that we study can be found in any number of references [9, 136, 209]. Briefly, we consider a periodic network of fuses arranged in a square lattice of size L tilted by 45° (the so-called 'diamond lattice', figure 1a). Each fuse is assigned a quenched current threshold from a common distribution with a cumulative distribution function $F(\cdot)$. If the current through a fuse exceeds its threshold, then the fuse is burned and is removed from the network i.e., its conductance is set to zero. The current through the network is ramped quasi-statically, and fuses are burned one at a time until the network becomes non-conducting, at which point the network is said to be fractured. We assign thresholds between 0 and 1, specifically we take $F(x) = x^\beta$, $\beta > 0$. This form of distribution of thresholds serves as model for a generic distribution with a power law tail at the origin, and has been studied widely [9, 136]. In this model the limit $\beta \to 0$ corresponds to infinite disorder, while the limit $\beta \to \infty$ corresponds to infinitesimal disorder. Figure 4.1 shows a schematic of an undamaged fuse network (4.1a), and realizations of fractured networks for various values of the parameter β. Notice how the damage looks percolation-like for small β while a single crack appears for large β.

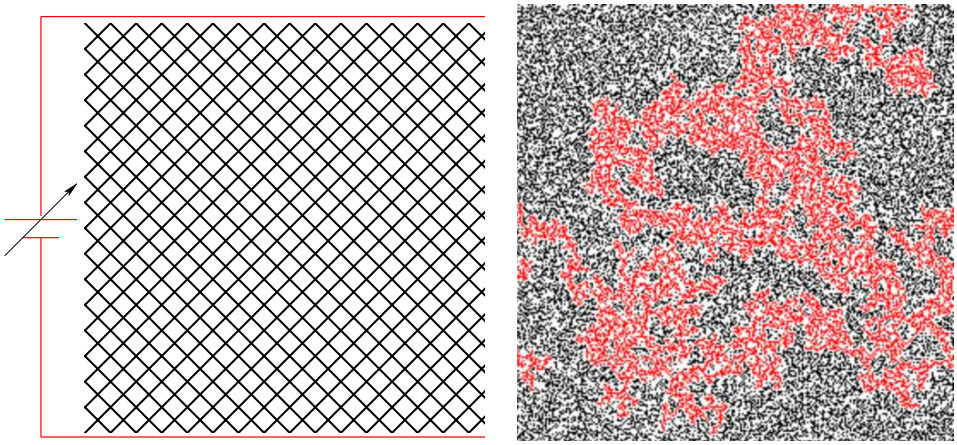

(a) A fuse network

(b) $\beta = 0.03$

(c) $\beta = 0.5$

(d) $\beta = 3.0$

Figure 4.1: **Fuse network model. a).** Schematic of a fuse network. Periodic boundary conditions are used in the horizontal direction. **b-d).** Fractured sample for various values of the parameter β; the spanning cluster (or crack) is colored red. There is a smooth crossover from percolation-like behavior for small β to nucleated cracks at large β.

4.4 Percolation and Cross-Over to Nucleation

We begin by arguing that crack-tip stress concentration is a relevant perturbation to the infinite disorder percolation critical point. Our assertion implies that percolation-like behavior is a finite-size crossover effect. We calculate self-consistent upper and lower bounds for the stress and damage fraction at failure, and show that all of these quantities vanish in the limit of large L. This will establish that percolation cannot be the dominant behavior for large L, since percolation demands that the damage fraction be finite. Let σ_f, ϕ_f be the stress and the damage fraction at failure, respectively. The lower bound on both quantities is trivially equal to 0. The upper bound is obtained self-consistently. Let us assume that $\phi_f < \phi_f^+ \ll 1$, where ϕ_f^+ is an upper bound on ϕ_f, and similarly $\sigma_f < \sigma_f^+ \ll 1$. Let, if possible, the damage be percolation-like, so that $\phi_f^+ = F(\sigma_f^+)$ [2]. The stress at the tip of a crack of length l (lattice units) is given by $\sigma_{tip}(l) \approx \sigma_f^+(1+\alpha\sqrt{l})$, where α is a lattice dependent constant. Thus, the length of a *critical crack* at a given stress and damage fraction is $l_{cr}(\sigma_f^+) \sim 1/(\sigma_f^+)^2\alpha^2 + \ h.o.t.$ The probability that a critical crack forms at a given lattice site is at least $F(\sigma_f^+)^{l_{cr}}$. Since there are L^2 sites in the lattice, the probability of 1 such crack appearing on the entire lattice is at least $L^2F(\sigma_f^+)^{l_{cr}}$ [108]. At the failure stress this probability is 1, thus σ_f^+ can be obtained by solving $L^2F(\sigma_f^+)^{l_{cr}(\sigma_f^+)} = 1$. It can be proved that the solution $\sigma_f^+(L) \to 0$ as $L \to \infty$, thus, $\phi_f^+ = F(\sigma_f^+) \to 0$.

We have established that percolation is unstable to nucleation, however, the crossover length is expected to be rather large. The reason for this effect is that $\phi_f^+(L)$ decays very slowly with L. The rate of decay obviously depends on $F(\cdot)$,

[2] A calculation based on effective medium theory yields $\phi = F(\sigma/(1-\phi^2)) \sim F(\sigma) + O(\sigma\phi^2)$. We ignore the higher order terms.

for $F(x) = x^\beta$ one can show that $\phi_f^+(L) \sim (\beta/2 \log L)^{\beta/2}$. More sophisticated estimates that account for stress concentration during the growth of the critical crack, as opposed to percolation-like growth assumed here, yield similar results. The convergence becomes extremely slow as β approaches 0, meaning that percolation threshold will be reached before nucleation of the critical crack for increasing larger system sizes. This is consistent with the previous studies that found that the fuse network can be mapped onto a percolation problem in the limit of $\beta \to 0$ [9]. However, one should note the subtle point that order of limits matters since percolation is ultimately unstable to nucleation at any β.

4.5 Mean-Field Model of Avalanches

The avalanche behavior associated with fracture can be understood via a simple model. The model and the associated analysis is valid in the vicinity of the critical point and breaks down for very large L. Consider an avalanche that starts with a bond breaking at a stress σ ($\ll 1$) and damage fraction ϕ ($\ll 1$). Linear elasticity predicts that the change in the stress field due to the breaking of the bond, $c(r, \sigma)$, decays as $c(r, \sigma) \sim \sigma/r^2$ (ignoring the dipolar directional dependence), where r is distance from the broken bond. The probability that a bond at distance r breaks in response to this change in stress is approximately given by $F'(\sigma)c(r, \sigma)$. Thus, the expected number of bonds that break in response to stress change due to one bond breaking is given by $\lambda \sim \int_1^L r dr F'(\sigma)c(r, \sigma) \sim F'(\sigma)\sigma \log L$. Substituting the form $F(x) = x^\beta$ gives $\lambda(\sigma, \beta, L) \sim \beta\sigma^\beta \log L = \beta\phi \log L$. This shows that $\lim_{\beta\to 0} \lambda(\beta, \phi, L) = 0$ (for fixed L), thus there are no avalanches for small β, and the damage is percolation-like. For suitable β the avalanche progresses as a branching process, where breaking

of one bond triggers a few more and so on (λ is also known as the branching ratio). It is well known that integrated avalanche size distribution for such processes is a power law with exponent $\tau_a = 3/2 + 1 = 5/2$; for suitably large L we expect the avalanche size distribution to be a power law with exponents consistent with the mean field value of $5/2$ [3]. Finally, for very large L (or β), the system flows away from the critical point and the avalanches get cutoff due to nucleation effects.

4.6 Scaling Functions and Renormalization Group

All the ideas discussed so far can be encapsulated neatly in the form of crossover scaling functions. The scaling form for the cluster size distribution can be derived by using ideas of scale invariance. Let $G(z_1, \ldots, z_n)$ be a scale invariant function, then by definition, $G(\cdot)$ should remain invariant under a rescaling by a factor b, i.e. $G(z_1, \ldots, z_n) = b^{\alpha_0} G(z_1 b^{\alpha_1}, \ldots, z_n b^{\alpha_n})$ for some constants α_i. Taking $b = 1 + \epsilon$ and solving up to first order in ϵ gives the general form of a scale invariant function as $G(z_1, \ldots, z_n) = z_1^{-\alpha_0/\alpha_1} \mathcal{G}(z_2 z_1^{-\alpha_2/\alpha_1}, \ldots, z_n z_1^{-\alpha_n/\alpha_1})$, where the universal scaling function, $\mathcal{G}(\cdot)$, and the critical exponents, α_i/α_1, are characteristic of the critical point [4], [220]. The variables z_i represent directions in parameter space near the critical point. The directions with $\alpha_i > 0$ belong to the *relevant parameters* and those with $\alpha_i < 0$ to *irrelevant parameters*. We treat $\beta, 1/L$ to be a relevant parameters, and let u be the leading irrelevant parameter (the largest of

[3] It is an interesting question as to where the numbers $3/2$ and $5/2$ appear from. While there is no simple explanation (I think), one can read a mathematical proof of these facts in Ref. [219].

[4] Other orderings of variables are equally valid, such as $G(z_1, \ldots, z_n) = z_2^{-\alpha_0/\alpha_2} \mathcal{G}_2(z_1 z_2^{-\alpha_1/\alpha_2}, \ldots, z_n z_2^{-\alpha_n/\alpha_2})$, etc. See [220] for details.

the negative α_i). Thus, ignoring all irrelevant variables but the leading one, the scale invariant distribution of cluster sizes can be written as

$$P_c(s_c|\beta, L) = s_c^{-\tau_c}\mathcal{F}_c\left(\beta L^{1/\nu_f}, s_c L^{-1/\sigma_c\nu_f}, uL^{-\Delta_f/\nu_f}\right) \tag{4.1}$$

where we use s as a generic variable for the distribution of sizes, the subscript c denotes variables associated with the clusters (the subscript a will be used to distinguish avalanches size distributions from the cluster sizes). We use the subscript f (for fracture) to distinguish the critical exponents from their counterparts in percolation theory. We know that in the limit of $\beta \to 0$ (at fixed L) the cluster size distribution should reduce to distribution of percolation clusters at the critical point, thus we can deduce two critical exponent combination, namely $\tau_c = 187/91 = 2.0549$ and $\sigma_c\nu_f = 48/91 = 0.5275$. In principle, Δ_f can also be related to percolation critical exponents, however, the corresponding exponent combination for percolation is not known, thus the mapping is not of much practical use. The moments of the cluster size distribution should scale as (treating u as a constant and taking a Taylor expansion for large L)

$$\langle s_c^n\rangle = L^{(n+1-\tau_c)/\sigma_c\nu_f}\left(\mathcal{J}_n^c(\beta L^{1/\nu_f}) + L^{-\Delta_f/\nu_f}\mathcal{K}_n^c(\beta L^{1/\nu_f})\right), \tag{4.2}$$

where $\mathcal{J}_n^c(\cdot)$, $\mathcal{K}_n^c(\cdot)$, $n = 2, 3\ldots$, are universal scaling functions [5]. From a data fitting perspective, it is easier to deal with the moments (as opposed to the distribution function) because $\mathcal{J}_n^c(\cdot)$, $\mathcal{K}_n^c(\cdot)$ are functions of just one scaling variable. The functions for the avalanche size distribution are completely analogous,

$$P_a(s_a|\beta, L) = s_a^{-\tau_a}\mathcal{F}_a\left(\beta L^{1/\nu_f}, s_a L^{-1/\sigma_a\nu_f}, uL^{-\Delta_f/\nu_f}\right), \tag{4.3}$$

$$\langle s_a^n\rangle = L^{(n+1-\tau_a)/\sigma_a\nu_f}\left(\mathcal{J}_n^a(\beta L^{1/\nu_f}) + L^{-\Delta_f/\nu_f}\mathcal{K}_n^a(\beta L^{1/\nu_f})\right), \tag{4.4}$$

where τ_a is expected to be close to its mean field value of $5/2$.

[5] This scaling relation is valid only if $n + 1 - \tau_c > 0$; we find $\tau_c = 187/91$, thus, $n \geq 2$.

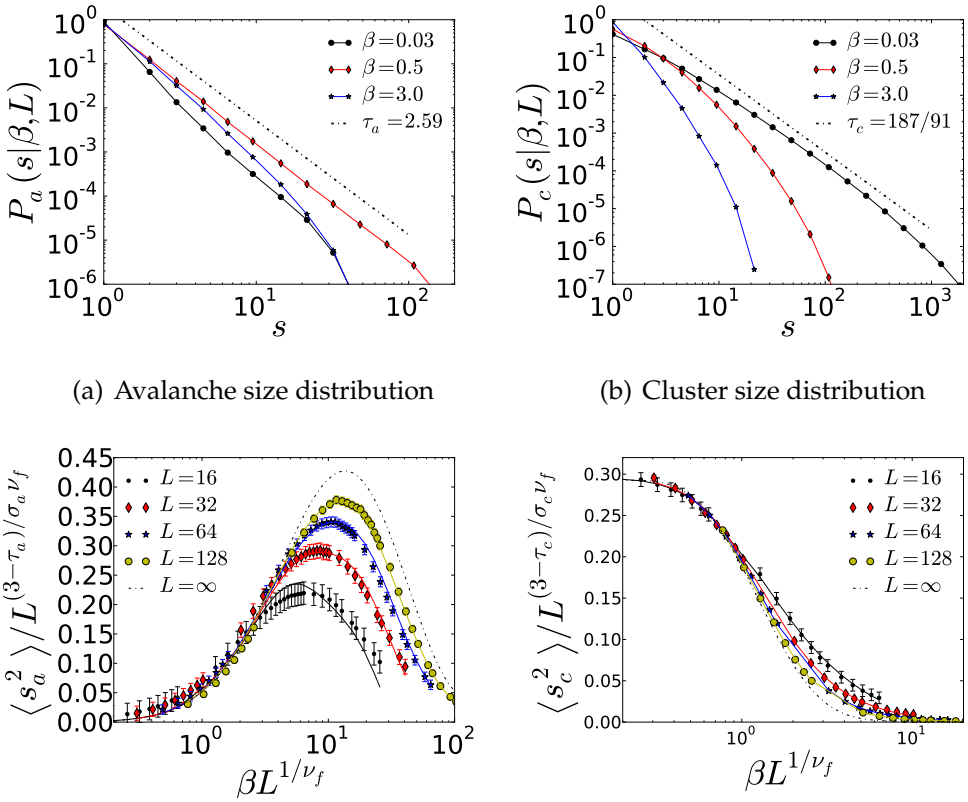

(a) Avalanche size distribution

(b) Cluster size distribution

(c) Scaling collapse of $\langle s_a^2 \rangle$

(d) Scaling collapse of $\langle s_c^2 \rangle$

Figure 4.2: **Scaling theory of fracture. a).** The avalanche size distribution shows a power law consistent with the mean field exponent of 5/2 for moderate β (= 0.5 at L = 128). As expected, the power law is distorted for much smaller or larger β. **b).** The cluster size distribution shows a power law that is consistent with the exponent predicted by percolation theory (= 187/91). The power law cutoff becomes smaller as one moves away from the critical point. **c, d).** The scaling forms fit the data well, confirming the predictions of the scaling theory. Higher moments of the distributions fit the scaling forms as well (not shown here). Notice the significant finite-size effects as the data gets closer to the $L = \infty$ curve (obtained by extrapolating the fit to the infinite size limit) with increasing system sizes.

4.7 Numerical Validation

We have done numerical simulations to verify our theoretical predictions. We did extensive statistical sampling of systems of size up to $L = 128$ and β between 0.03 and 8. In order to fit the data to the scaling predictions we use the following functional forms for the scaling functions for the moments of the cluster size distribution (with $y_c(x) \equiv (\log x - \mu_c)/\alpha_c$)

$$\mathcal{J}_n^c(x) = a_{0,n}\mathrm{erf}\left(y_c(x)\right) + e^{-(y_c(x))^2} \sum_{i=0}^{i=m} A_{i,n}^c H_i\left(y_c(x)\right), \tag{4.5}$$

$$\mathcal{K}_n^c(x) = a_{1,n}\mathrm{erf}\left(y_c(x)\right) + e^{-(y_c(x))^2} \sum_{i=0}^{i=m} B_{i,n}^c H_i\left(y_c(x)\right), \tag{4.6}$$

where μ_c, α_c, $a_{0,n}$, $a_{1,n}$, $A_{i,n}^c$, $B_{i,n}^c$ are fitting parameters, $\mathrm{erf}(\cdot)$ is the error function, and $H_i(\cdot)$ is the i^{th} Hermite polynomial. We use the first three Hermite polynomials in the expansion, i.e., $m = 3$. The corresponding forms for the avalanches are (with $y_a(x) \equiv (\log x - \mu_a)/\alpha_a$)

$$\mathcal{J}_n^a(x) = e^{-(y_a(x))^2} \sum_{i=0}^{i=m} A_{i,n}^a H_i\left(y_a(x)\right), \tag{4.7}$$

$$\mathcal{K}_n^a(x) = e^{-(y_a(x))^2} \sum_{i=0}^{i=m} B_{i,n}^a H_i\left(y_a(x)\right). \tag{4.8}$$

The forms of the scaling functions are chosen so that they have the correct asymptotic behavior. As discussed previously, we need that $\lim_{\beta L^{1/\nu_f}\to 0,\infty} \mathcal{J}_n^a(\beta L^{1/\nu_f}) = 0$ since there are no avalanches for very small β (at fixed L) and at very large L (at fixed β). On the other hand we need $\lim_{\beta L^{1/\nu_f}\to 0} \mathcal{J}_n^c(\beta L^{1/\nu_f}) = C$, for some constant C (according to percolation theory) and $\lim_{\beta L^{1/\nu_f}\to \infty} \mathcal{J}_n^c(\beta L^{1/\nu_f}) = 0$ since there are no clusters in the nucleation dominated regime away from the critical point. The forms used here satisfy all these requirements.

Figure 4.2 shows the size distributions as well as fits to the scaling forms. It

is evident that the data is consistent with the scaling theory. Based on joint fits for $n = 2,\ 3$ ($n = 3$ not shown in figure 4.2) we estimate the following values of the critical exponents: $\nu_f = 1.49 \pm 0.20$, $\tau_a = 2.59 \pm 0.15$, $\sigma_a = 0.45 \pm 0.15$, $\Delta_f = 1.12 \pm 0.30$, $\sigma_c = 0.35 \pm 0.07$. The scaling exponent τ_c, and the exponent combination $\sigma_c \nu_f$ are held at their theoretical values of 187/91 and 48/91, respectively, and τ_a is found to be close to its mean field value of 5/2. The statistical error bars are much smaller than the error bars reported here. We have estimated the error bars due to systematic errors by using a variety of techniques such as varying the number of terms in the scaling functions, trying different fitting forms, varying the critical range for the fits, varying the error bars on the data over a reasonable range, etc.

4.8 An Unusual Critical Point and Phase Diagram

Figure 4.3 shows the phase diagram that emerges from our analysis. In the $\beta - 1/L$ space, curves along which the scaling variable $\beta L^{1/\nu_f}$ attains a critical value demarcate the boundary between qualitatively different behavior. Note that the exact position of the boundaries is somewhat arbitrary, since this is a not an abrupt (first order) transition; however, the diagram is qualitatively accurate.

The critical phenomena associated with fracture has several intriguing characteristics. Firstly, the scaling function associated with the avalanches has a singularity at 0, $\lim_{\beta L^{1/\nu_f} \to 0} \mathcal{J}_n^a(\beta L^{1/\nu_f}) = 0$, that subdues the avalanche behavior as the critical point is approached (this corresponds to, say, taking the limit of large L at fixed, but small, β, and entering the "nucleation" regime of Fig. 4.3). Secondly, there is no point in the phase diagram (except for the physically un-

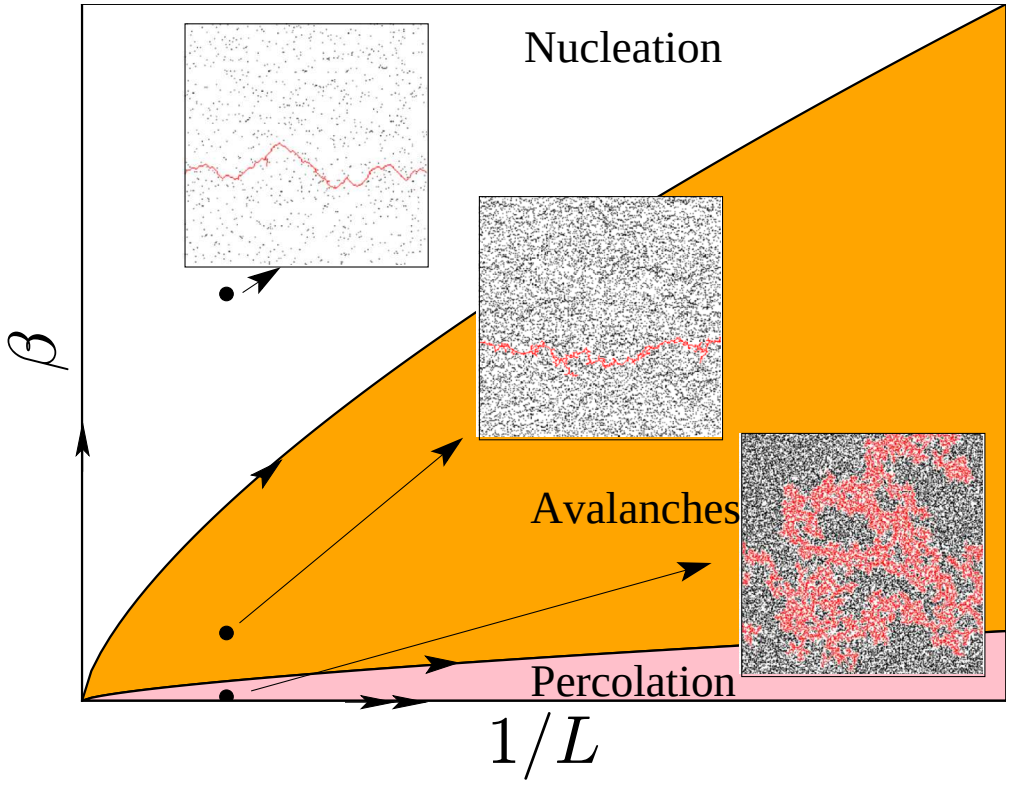

Figure 4.3: **Phase diagram for brittle fracture in disordered media.** Disorder decreases along the β axis; nucleation governs the behavior for small disorder or long length scales. Percolation is characteristic of the large disorder regime, while the crossover region exhibits interesting critical behavior in the form of scale free distributions of avalanche sizes. The topology of the fractured samples evolves from percolation-like damage for large disorder to well defined sharp cracks in the nucleated regime. The phase boundaries are quantitatively somewhat arbitrary, and are set at the value of the scaling variable $\beta L^{1/\nu_f}$ at which the second moment of the avalanche size become half of its peak value (for the avalanche phase); the boundary of the percolation phase is found analogously.

realizable $\beta = 0$ limit) that shows any critical phenomena in the limit of $L \to \infty$. Thus, scale invariance itself becomes a finite-size effect; perhaps this phenomena should be named *finite-sized criticality*. Finally, it is rather remarkable that the critical phenomena (typically associated with continuous phase transitions) gives way to nucleation (a first order transition) in the limit of long length scales! Thus, fracture has mixed first order and continuous transition character. Notice that the reason that the critical phenomena gives way to nucleation is that in the limit of large L the failure stress σ_f goes to zero, and so does the amount of distributed damage ϕ_f. Transitions of mixed first order and continuous character have become somewhat of a mini theme in the past decade or so. Recently we noted that the Mott transition and dielectric breakdown have a mixed character [221]; similar findings have been reported in a variety of fields such as jamming transitions, rigidity percolation [222], and phase-separated manganites [223].

4.9 Conclusion

In conclusion, we have presented a scaling theory of fracture that builds on renormalization group ideas and unifies several disparate results in the field. Our theory shows that percolation-like behavior as well as the scale invariant precursor avalanches leading to fracture are finite-size effects. We show that on long length scales brittle fracture is always nucleated. We hope that our analysis will pave the way for a deeper understanding of the many mysteries associated with the phenomenon of fracture.

APPENDIX A

APPENDIX

This appendix gives a short introduction to various results and mathematical tools needed to better understand the content of this thesis.

A.1 Extreme Value Statistics

Extreme value statistics is a branch of classical statistics. Chapter 1 of this thesis assumes a knowledge of the basic results from extreme value statistics that are discussed here. Extreme value statistics is the study of distribution of the largest or the smallest element of a set of independent and identically distributed random variables. Let X_i, $i = 1, \ldots, n$ be i.i.d random variables with a distribution function $F(\cdot)$. Let $Z_n = \max_{i=1,\ldots,n} X_i$, then the distribution of Z_n is given by

$$H_n(z) = P(Z_n < z) = F(z)^n. \tag{A.1}$$

Clearly, $H_n(\cdot)$ does not have a meaningful limit for large n. We call a distribution $F(\cdot)$ max-stable if there exist constants A_n and B_n such that the limit $\lim_{n\to\infty} F^n(A_n z + B_n)$ exists. If this limit exists, then the central theorem of extreme value statistics asserts that it has to be of the following form

$$\lim_{n\to\infty} F^n(A_n z + B_n) = G_\gamma(z) = \exp\left\{-(1+\gamma z)^{-1/\gamma}\right\}, \quad \gamma \in \Re, 1 + \gamma z > 0. \tag{A.2}$$

If A.2 holds, then $F(\cdot)$ is said to be in the domain of attraction of $G_\gamma(\cdot)$. Notice that so far I have formulated the theory in terms of maximum of random variables, however, in fracture one deals with minimum of random strengths, as opposed to maximum. There is a way to translate between the two, since

$$\min_{i=1,\ldots,n} X_i = -\max_{i=1,\ldots,n} -X_i. \tag{A.3}$$

Further, one can arrive at the limit results directly, let $Y_n = \min_{i=1,\ldots,n} X_i$, then the distribution of Y_n is given by

$$J_n(z) = P(Y_n < z) = 1 - (1 - F(z))^n, \tag{A.4}$$

and the limit for min-stable distributions is

$$\lim_{n\to\infty} J_n(A_n z + B_n) = G^*_\gamma(z) = 1 - G_\gamma(-z). \tag{A.5}$$

A distinction is often drawn between the cases for $\gamma > 0$, $\gamma < 0$, and $\gamma = 0$. In the statistics literature these are called the Type I, Type II and Type III distributions, respectively. In physics literature they are called the Fréchet, the Weibull, and the Gumbel distributions. The convergence to limit forms is rather remarkable in that it asserts that the limit form $G_\gamma(\cdot)$, if it exists, bears little resemblance to $F(\cdot)$. When does this remarkable result hold? There are several characterizations of the "domain of convergence", I state one of them that is particularly concise. Let us define a function $f(\cdot)$

$$f \equiv \left(\frac{-1}{\log F}\right)^{\leftarrow}, \tag{A.6}$$

i.e., $f(\cdot)$ is the left continuous inverse of $-1/\log F(\cdot)$. Then, the following is a necessary and sufficient condition for A.2 to hold

$$\lim_{t\to\infty} \frac{f(tz) - f(t)}{t f'(t)} = \frac{z^\gamma - 1}{\gamma}, \tag{A.7}$$

while the following is a sufficient condition

$$\lim_{t\to\infty} \frac{f'(tz)}{f'(t)} = z^{\gamma-1}, \tag{A.8}$$

It is worth mentioning that the theory of extreme value statistics is very closely related to the theory of regularly varying functions, and the reader will be well

advised to gain familiarity with the topic. In general, a function $r(\cdot)$ is said to be regularly varying at ∞ (or 0) with an index k if

$$\lim_{t\to\infty} \frac{r(tz)}{r(t)} = z^k. \tag{A.9}$$

All polynomials are regularly varying, z^k is the canonical k-varying function. Note that the sufficient condition for domain of convergence is stating that $f'(\cdot)$ is regularly varying with index $\gamma - 1$. It can be shown that any regularly varying function can be expressed as $r(z) = z^k L(z)$, where $L(\cdot)$ is *slowly varying*, meaning

$$\lim_{t\to\infty} \frac{L(tz)}{L(t)} = 0. \tag{A.10}$$

The theory of extreme value statistics shows that the limit distributions of the extremes are universal (up to the parameter γ). What about the rate of convergence to the limit forms? The two main characterizations of the approach to the limit form are studied in the theory of large deviations, and the theory of Edgeworth type expansions. Here I state a result on the Edgeworth expansions that is due to de Haan and Resnick. It will be seen that the rate of convergence is closely related to regularly varying functions. The result due to de Haan and Resnick is stated below

$$\lim_{n\to\infty} \frac{F^n(A_n z + B_n) - G_\gamma(z)}{R(n)} = \left(-\log G_\gamma(z)\right)^{(1+\gamma)} G_\gamma(z) H_\gamma\left(-\log(-\log G_\gamma(z))\right), \tag{A.11}$$

where $R(\cdot)$ is defined as

$$R(n) \equiv \frac{n f''(n)}{f'(n)} - \gamma + 1, \tag{A.12}$$

and $H_\gamma(\cdot)$ is defined as

$$H_\gamma(z) \equiv \begin{cases} \int_0^z e^{\gamma u} \int_0^u e^{\rho s} ds du, & \text{for } \gamma \geq 0 \\ -\int_z^\infty e^{\gamma u} \int_0^u e^{\rho s} ds du, & \text{for } \gamma < 0. \end{cases}$$

Finally, the constant ρ is the index of variation of $R(\cdot)$ at ∞ (it can be proved that $R(\cdot)$ is indeed regularly varying if $F(\cdot)$ is in the domain of attraction of $G_\gamma(\cdot)$),

$$\lim_{t\to\infty} \frac{R(tn)}{R(t)} = n^\rho. \tag{A.13}$$

The norming constants A_n, B_n given below are "optimal" in the sense that choosing another sequence will not result in an improvement in the rate of convergence

$$A_n = nf'(n), \quad B_n = f(n). \tag{A.14}$$

Are the domain of convergence and the rate of convergence related? It seems not. In fact, it can be shown that $f'(\cdot)$ is regularly varying with index $\gamma - 1$. Thus, it admits a representation of the form $f'(z) = z^{\gamma-1}L(z)$ for some slowly varying function $L(\cdot)$. Consider

$$R(n) = \frac{nf''(n)}{f'(n)} - \gamma + 1, \tag{A.15}$$

$$= \frac{(\gamma-1)n^{\gamma-1}L(n) + n^\gamma L'(n)}{n^{\gamma-1}L(n)} - \gamma + 1, \tag{A.16}$$

$$= \frac{nL'(n)}{L(n)}. \tag{A.17}$$

The slowly varying part of $f'(\cdot)$ that had a passive role to play in determining the domain of convergence has the leading role in deciding the rate of convergence. This indicates that the domain of attraction and the rate of convergence are independent properties. Indeed, the maximum of exponential random variables converges rather quickly to the Gumbel form ($R(n) \sim 1/2n$), while the maximum of normal random variables converges rather slowly to Gumbel ($R(n) \sim 1/\log n$). Similarly, the maximum of power-law distributed variables ($F(z) = 1 - z^{-\alpha}$) converges quickly to the Fréchet form ($R(n) \sim (2\alpha^2 - 3\alpha + 1)/2\alpha^2 n$), while maximum of variables with a slightly different distribution ($F(z) = 1 - z^{-\alpha}\log z$) converge only logarithmically.

A.2 Linear Elastic Fracture Mechanics

Linear elastic fracture mechanics is a vast field, worthy of several textbooks worth of discussion. Here I reproduce some very canonical results. Throughout I assume isotropic linear elastic behavior

$$\sigma_{ij} = \lambda \epsilon_{kk} \delta_{ij} + 2\mu \epsilon_{ij}, \tag{A.18}$$

where λ, μ are the Lame constants (μ is the same as the shear modulus G). The above relation can be inverted as

$$\epsilon_{ij} = -\frac{\nu}{E} \sigma_{kk} \delta_{ij} + \frac{1+\nu}{E} \sigma_{ij}, \tag{A.19}$$

where

$$\nu = \frac{\lambda}{2(\lambda+\mu)}, \quad E = \frac{\mu(3\lambda+2\mu)}{\lambda+\mu)}. \tag{A.20}$$

More generally one might write linear relation between stress and strain as $\sigma_{ij} = C_{ijkl} \epsilon_{kl}$, yielding a total of 81 elastic constants in 3 dimensions. However, general arguments show that C_{ijkl} must have the following symmetries

$$C_{ijkl} = C_{klij} = C_{jikl} = C_{ijlk}, \tag{A.21}$$

thus reducing the number of constants to 21. Finally, the requirements of isotropy reduce the number of constants to 2, the Lame constants.

The condition of equilibrium, ignoring body forces and inertial effects, is given by (a derivation of this basic equation can be found in any standard text on elasticity theory)

$$\sigma_{ij,j} = 0. \tag{A.22}$$

The notation $\sigma_{ij,j}$ is the Einstein notation, where a 'comma' denotes differentiation, and the repeated index is summed over. Thus, in 3 dimensions,

$$\sigma_{ij,j} \equiv \sum_{j=1,2,3} \frac{\partial \sigma_{ij}}{\partial x_j}, \tag{A.23}$$

and so Eq. A.22 is a vector equation saying that the tensor field σ_{ij} is divergence free. Several important results can be derived by using complex variables and analytic functions. In this formulation the displacements and stresses are expressed as functions of the complex variable $z = x + iy = re^{i\theta}$. There are several formulations of elasticity in terms of potential functions, I present the one due to Westergaard. In this formulation all problems of planar elasticity can be reduced to finding two complex potential functions $\Phi(\cdot)$ and $\Psi(\cdot)$. The state of stresses and displacements (and hence strains) can be written in terms of these functions

$$\sigma_x + \sigma_y = 2\left[\Phi'(z) + \overline{\Phi'(z)}\right], \tag{A.24}$$

$$\sigma_y - \sigma_z + 2i\tau_{xy} = 2\left[\overline{z}\Phi''(z) + \Psi'(z)\right], \tag{A.25}$$

$$2\mu(u + iv) = \kappa\Phi(z) - z\overline{\Phi'(z)} - \overline{\Psi(z)}, \tag{A.26}$$

where $u(z), v(z)$ are the real displacements, and

$$\kappa = \begin{cases} 3 - 4\nu, & \text{for plane strain,} \\ (3 - \nu)/(1 + \nu), & \text{for plane stress.} \end{cases}$$

This formulation can be further simplified in situations with more symmetry. In case of anti-plane shear just one complex potential, $\Omega(\cdot)$ is sufficient,

$$\tau_{xz} - i\tau_{yz} = \Omega'(z) \tag{A.27}$$

$$\mu w = \mathrm{Re}\Omega(z), \tag{A.28}$$

where w is the only non-zero component of the displacement (out of plane). The pure mode-I case (symmetric about x-axis) is given by $\Psi'(z) = -z\Phi''(z)$, while the

pure mode-II case (anti-symmetric about the x-axis) is given by $\Psi'(z) = -\Phi'(z) - z\Phi''(z)$. The potential functions $\Phi(\cdot)$ and $\Psi(\cdot)$ for several cases can be constructed by using the potential functions for distributed loading on the crack face in pure mode-I and mode-II. Let the loading on the crack face be $\mathbf{t} = p_2(x_1)\mathbf{e_2}$, then

$$\Phi'(z) = \frac{1}{2\pi\sqrt{z^2 - a^2}} \int_{-a}^{a} p_2(t) \frac{\sqrt{a^2 - t^2}}{z - t} dt, \tag{A.29}$$

while if $\mathbf{t} = p_1(x_1)\mathbf{e_1}$, then

$$\Phi'(z) = \frac{-i}{2\pi\sqrt{z^2 - a^2}} \int_{-a}^{a} p_1(t) \frac{\sqrt{a^2 - t^2}}{z - t} dt. \tag{A.30}$$

The singularity at the crack tip is characterized by the means of three stress intensity factors $K_I,\ K_{II}, K_{III}$, called the mode-I, mode-II and mode-III stress intensity factors, respectively. In a coordinate centered at the crack tip (with the y-axis pointing perpendicular to the crack front, and the z-axis parallel to it) , these are defined as

$$K_I \equiv \lim_{r\to 0} \sqrt{2\pi r}\sigma_{yy}, \quad K_{II} \equiv \lim_{r\to 0} \sqrt{2\pi r}\sigma_{xy}, \quad K_{III} \equiv \lim_{r\to 0} \sqrt{2\pi r}\sigma_{yz}, \tag{A.31}$$

where the factor $\sqrt{2\pi}$ is kept for historical reasons. Why is the singularity at the crack tip in the form of a square-root? We will soon show that this is (almost) generic. The stress intensity factors for the distributed mode-I and mode-II loadings discussed earlier can be found to be

$$K_I = \frac{1}{\sqrt{\pi a}} \int_{-a}^{a} p_2(t) \sqrt{\frac{a + t}{a - t}} dt, \tag{A.32}$$

$$K_{II} = \frac{1}{\sqrt{\pi a}} \int_{-a}^{a} p_1(t) \sqrt{\frac{a + t}{a - t}} dt. \tag{A.33}$$

To understand the origin of the square root singularity, consider the problem of a semi-infinite crack in an infinite medium A.1. The boundary value problem

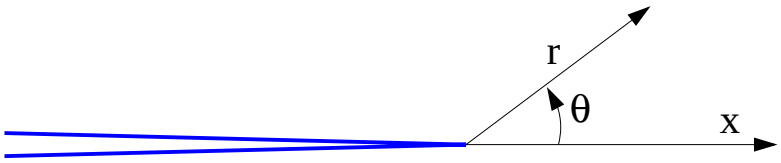

Figure A.1: Polar coordinates at a sharp crack tip. The $\theta = 0$ direction is aligned with the crack, while $\theta = \pm\pi$ gives the two crack surfaces that are assumed to extend indefinitely (marked in bold blue color).

for this case is $\sigma_{ij,j} = 0$, and along the crack faces $\theta = \pm\pi$ we need $\sigma_{\theta\theta} + i\sigma_{r\theta} = 0$. Assuming potentials of the form $\Phi(z) = Az^{\lambda}, \Psi(z) = Bz^{\lambda}$ one can show that the most general solution is of the form

$$\sigma_{ij} = \sum_{n=-\infty}^{\infty} r^{(n+1)/2} \hat{\sigma}_{ij}(\theta). \tag{A.34}$$

The lowest order pole in this series is due to the $r^{-1/2}$ term. There is a region where this term dominates over the next (non-singular) terms. The far-field solution is given by the non-singular terms, while the structure of the defect-core (near crack-tip) is dominated by the more singular terms ($r^{-3/2}$ etc.). There is an intermediate region where the solution is determined by the $r^{1/2}$ term, and this is the region of interest since it is neither effected by the boundary conditions at infinity, nor by the non-linearities and other details near the crack-tip. This is the universal part of the elastic field due to a crack. Thus, the crack field is characterized in terms of the stress intensity factors which are normalized so as to capture the magnitude of the $r^{-1/2}$ singularity. The stress field due to a crack-tip is generically written as

$$\sigma_{ij} = \frac{1}{\sqrt{2\pi r}} \left(K_I \sigma_{ij}^{I}(\theta, \phi) + K_{II} \sigma_{ij}^{II}(\theta, \phi) + K_{III} \sigma_{ij}^{III}(\theta, \phi) \right). \tag{A.35}$$

It should be noted that there are situations where the crack tip singularity is not of the type $r^{-1/2}$. These include blunt cracks, wedge cracks or intersections of cracks with free surfaces etc.

A.3 Griffith's Theory of Crack Growth

Griffith's theory is based on thermodynamic ideas of energy balance. The suggestion is the calculate the energy change due to infinitesimal growth of a crack. If this change is negative, i.e., if the crack propagation lowers the net energy of the system then it is a thermodynamically favorable change and will occur spontaneously. There are several methods (and model systems) to do such calculations; here I present two. All of them yield similar results, up to some details. The energy criteria is

$$d\Pi^{int} + d\Pi^{ext} + d\Gamma \leq 0, \tag{A.36}$$

where Π^{int} is the potential due to the elastic energy stored in the system, Π^{ext} is the potential due to the work done by external forces, and Γ is the surface energy of the crack surface. For a mode-I crack of length $2a$ with a far field stress σ_∞ these quantities are

$$\Pi^{int} + \Pi^{ext} = -\sigma_\infty^2 a^2 \pi \frac{1+\kappa}{8G}, \quad \Gamma = 4a\gamma, \tag{A.37}$$

where γ is the surface energy per-unit length (we assume unit thickness). Taking the variation with a, the criteria for crack growth reads

$$\frac{d(\Pi + \Gamma)}{da} \leq 0. \tag{A.38}$$

Thus, a crack of length $2a$ becomes unstable if

$$\sigma_{cr}\infty \geq \sqrt{\frac{16G\gamma}{\pi(1+\kappa)a}}, \tag{A.39}$$

and conversely, given a far-field stress of σ_∞ the critical crack length needed to create an unstable crack is

$$a_{cr} = \frac{16G\gamma}{\pi(1+\kappa)\sigma_\infty^2}. \tag{A.40}$$

It is generically true that the critical crack length scales as $1/\sigma^2$. The quantity $d\Pi/da$ is often called the elastic energy release rate, where $\Pi = \Pi^{int} + \Pi^{ext}$. More generally, one can show that

$$\mathcal{G} \equiv -\frac{d\Pi}{da} = \frac{1+\kappa}{8G}(K_I^2 + K_{II}^2) + \frac{1}{2G}K_{III}^2. \tag{A.41}$$

The criteria for crack growth initiation can then be written as

$$\mathcal{G} = \mathcal{G}_{cr}. \tag{A.42}$$

This criteria is known as the Griffith's criteria. More specifically, The parameter $\mathcal{G}_{cr}$ is called the *crack resistance*, and is a material property. Griffith choose $\mathcal{G}_{cr}$ to be exactly equal to the surface energy needed to the create the incremental crack area. Note that even if the material is isotropic, $\mathcal{G}_{cr}$ can have a directional dependence due to the crystal structure. Equation A.41 is sometimes written in terms of the parameters E, ν. For the case of plain strain it becomes

$$\mathcal{G} = \frac{1-\nu^2}{E}(K_I^2 + K_{II}^2), \tag{A.43}$$

while for the case of plain stress it becomes

$$\mathcal{G} = \frac{1}{E}(K_I^2 + K_{II}^2) + \frac{1+\nu}{4E}K_{III}^2. \tag{A.44}$$

Note that the Griffith's criteria is a necessary condition for crack propagation, but it might not be sufficient. In ductile materials a lot more energy is dissipated in the plastic zone due to plastic deformations than is needed to create the material surface. This can lead to a blunting of crack tip and ultimate arrest of the growing crack. Thus, ductile materials are tougher than the Griffith prediction. In such cases the parameter $\mathcal{G}_{cr}$ is taken to include all the energy dissipated in the plastic deformation, surface creation, and any other processes that occur near the crack tip.

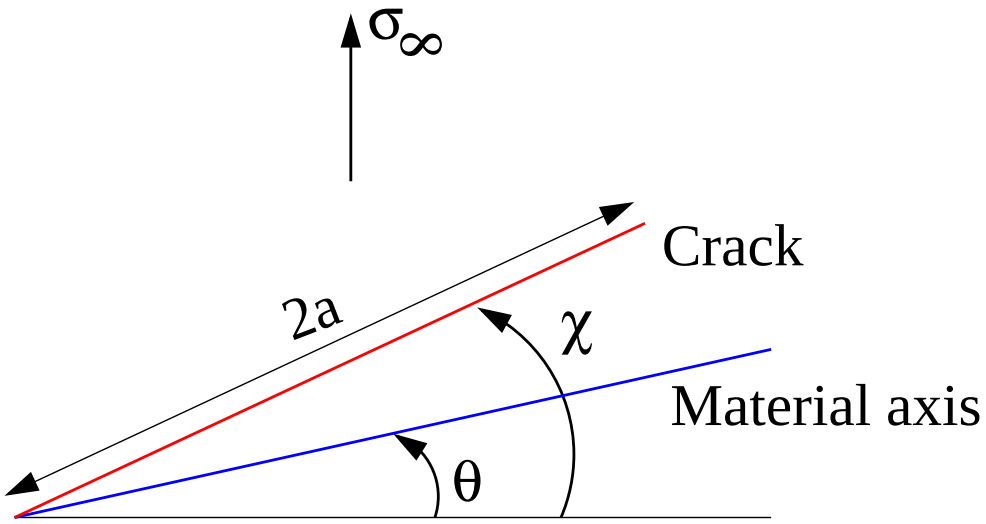

Figure A.2: A straight crack of length $2a$ (drawn in red) at an angle χ to the pure mode-I direction. The material axis is at an angle θ to the pure mode-I direction.

A.4 Crack Paths in Crystalline Materials

The celebrated principle of local symmetry predicts that in an isotropic material, cracks will grow in a direction that corresponds to a local mode-I field at the crack front ($K_{II} = 0$). Does this criteria generalize to cases where the isotropy is broken by the presence of a crystal lattice and cleavage planes? Experimental and numerical evidence suggests that it does not. A number of "principles" or criteria have been suggested in order to predict the crack growth direction in such cases. I will study the validity of such criteria by using classical molecular dynamics simulations of graphene. This study is motivated by recent experiments conducted by Zenghui Wang and Jiwoong Park at Cornell.

Consider the system shown in figure A.2. The direction of pure mode-I growth is perpendicular to the loading direction. The principle of local symmetry would predict that a crack would grow in this direction (i.e. $\chi = 0$). Let

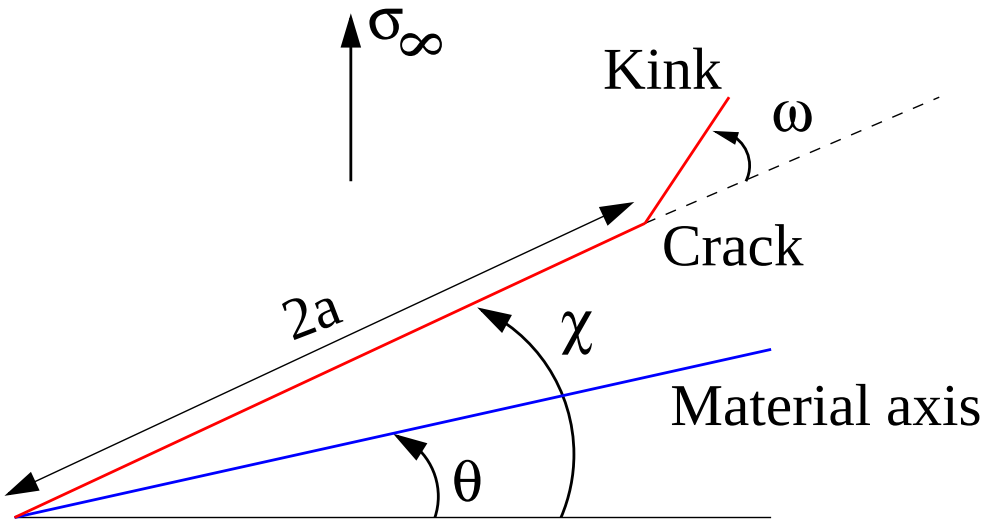

Figure A.3: Crack with an infinitesimal kink developing at an angle ω to the crack.

us assume that even though the material is linear isotropic, the surface energy $\gamma(\cdot)$ has a directional dependence, with $\gamma(0)$ being the energy of a unit surface along the material axis. Let the material axis be at an angle θ to the pure mode-I direction. In what direction χ is the crack growth stable? To answer this question, let us assume that instability appears in the form of an infinitesimal kink at the crack tip, as shown in Fig. A.3. The direction of stable growth is one in which the most favorable kink happens at $\omega = 0$, where ω is the angle that the kink makes with the main crack. In other words, the stable direction of crack growth is the one that is immune to instabilities, and cracks growing in this direction do not curve during their growth. It is well known that principle of local symmetry and the principle of maximum hoop-stress give $\chi = 0$ as the direction of stable growth. However, they do not account for crystalline anisotropy.

Let $\mathcal{H}$ be the net energy release rate (elastic and surface), then it can be demonstrated that for plane strain and up to the first order in ω

$$\mathcal{H} = \frac{1-\nu^2}{E}(K_I^2 + K_{II}^2 - 2K_I K_{II}\omega) - 2\gamma\,(\chi + \omega - \theta)\,. \tag{A.45}$$

The stress intensity factors K_I, K_{II} are solutions of complicated boundary value problems, and can be evaluated in closed form for only a handful of situations. In order to make progress, we assumes that we are interested only in finite cracks in infinite plates as shown in Fig. A.3. For this case we can use the techniques of complex variables discussed earlier to get

$$\frac{K_I}{\sigma_\infty \sqrt{a\pi}} = \cos^2\chi, \quad \frac{K_{II}}{\sigma_\infty \sqrt{a\pi}} = \cos\chi \sin\chi. \tag{A.46}$$

Let us generalize the principle of maximum energy release rate to mean that a crack grows in the direction that maximizes the net energy release rate $\mathcal{H}$. Further, for stability we need that crack should not kink, or $\omega = 0$. Thus, we have

$$\left.\frac{d\mathcal{H}}{d\omega}\right|_{\omega=0} = 0, \quad \left.\frac{d^2\mathcal{H}}{d\omega^2}\right|_{\omega=0} < 0, \quad \mathcal{H}(\omega = 0) \geq 0. \tag{A.47}$$

Do these calculations based on continuum and equilibrium ideas give realistic predictions for crack paths? We test these theories by comparing their predictions to crack paths observed in molecular dynamics simulations of graphene. All simulations are performed in the canonical (NVT) ensemble by using Nose-Hoover style non-Hamiltonian equations of motion implemented in the freely available software LAMMPS [224]. A time step of 0.1 femtoseconds is used in all simulations. The simulations are conducted at a range of temperatures varying from 0-1000 K, even though most simulations reported here are either at 10K or 300K, as these two temperatures were representative of the low and high temperature behavior of the system. The simulation is set up by introducing a notch of length 20 Angstroms in a sheet of graphene that has been stretched uniformly in the *y*-direction as shown in figure A.4. Fixed boundary conditions are used in the *y*-direction, while the boundaries in the *x*-direction are free.

I will report the observed behavior for two potentials, namely, AIREBO [225]

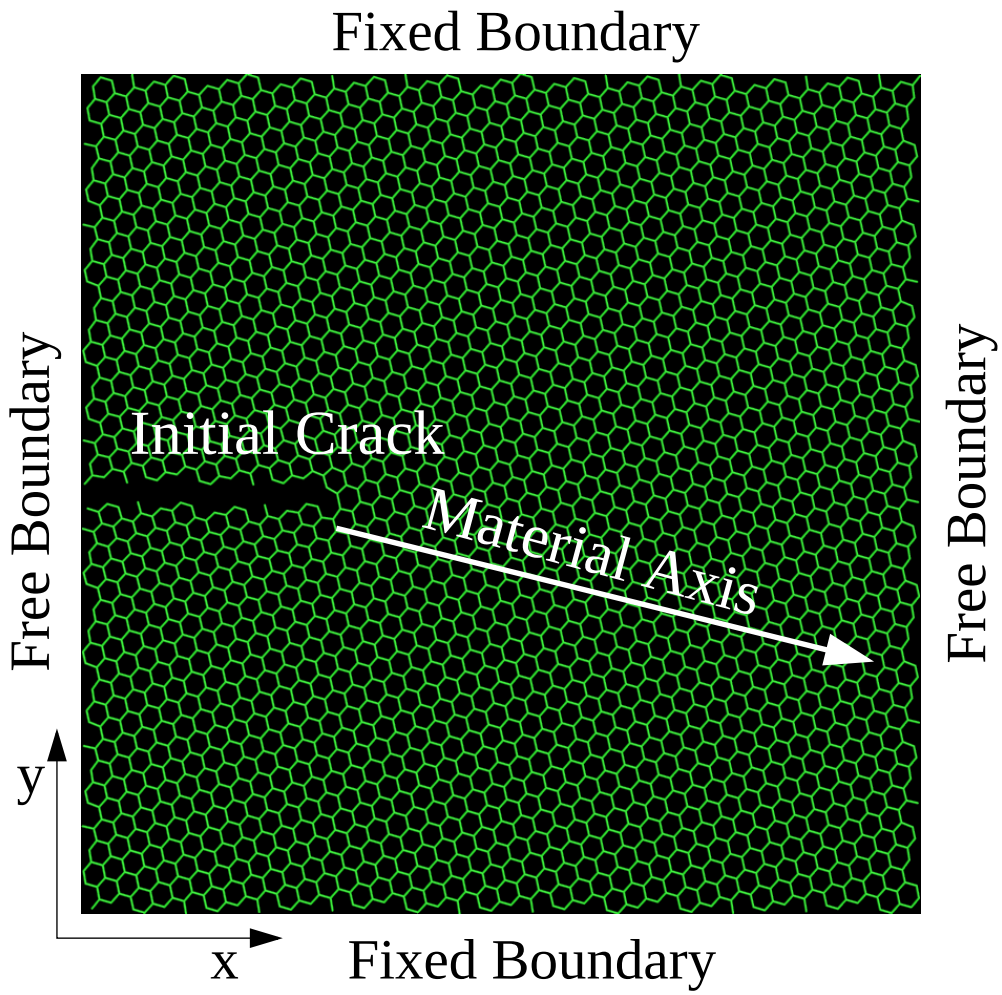

Figure A.4: Simulation setup with free and fixed boundary conditions.

and LCBOP [226] (Reaxff [227] yields similar results for the two different parameterizations [228, 229] that I have tested). I will also study the behavior of AIREBO as a parameter r_{cc} [230] is varied. This parameter represents the lower cut-off distance in a switching function to model the C-C bond breakage.

In order to get a prediction from Eq. A.47, the surface energy per-unit length, $\gamma(\cdot)$, is needed as an input. The surface energy can be readily calculated on a computer (it is much harder to measure experimentally). The basic idea is that

the net energy of a strip of graphene (or any other material) is given by

$$E_{net} = E_{bulk} + E_{edge} = ne_b + l\gamma,$$

where n is the number of atoms in the strip, e_b is the ground state energy per-atom in the bulk, and l is the net length of the exposed edge. This equation can be used to calculate the surface energy per-unit length, since E_{net} and e_b are trivial to measure for a given configuration and a given atomistic potential. This process is described in detail in Ref. [231]. Further, the authors there give a rather simple formula for the edge energy as a function of the angle α of the edge with respect to the armchair axis of graphene

$$\gamma(\alpha) = 2\gamma_a \sin(\pi/6 - \alpha) + 2\gamma_z \sin(\alpha), \tag{A.48}$$

where γ_a, γ_z are the energies of the armchair and the zigzag edges, respectively. The edge energy has the obvious symmetries $\gamma(\alpha) = \gamma(-\alpha)$ and $\gamma(\alpha) = \gamma(\pi/3 - \alpha)$. Figure A.5 shows the comparison of the numerical results with the prediction. For the AIREBO potential the maximum relative error is 1.6% or 0.02 eV/Å, while for the LCBOP potential it is 0.7% or 0.007 eV/Å, thus the formula works fairly well.

Figure A.6 shows a plot of the maximum stable crack angle, χ_{max}, as a function of the orientation of material axis with respect to the loading. Notice that when either the armchair axis is almost perpendicular to the loading direction ($\theta \sim 0$), or when the zigzag axis is almost perpendicular to the loading direction ($\theta \sim 30^\circ$), the crack deflection is at most equal to the misalignment. Thus, for small misalignments, the prediction is that the crack should tend to propagate along the closest high symmetry direction.

One can foresee that the predictions of the simple minded theory discussed previously is doomed to fail. The most obvious reason is that the entire theory

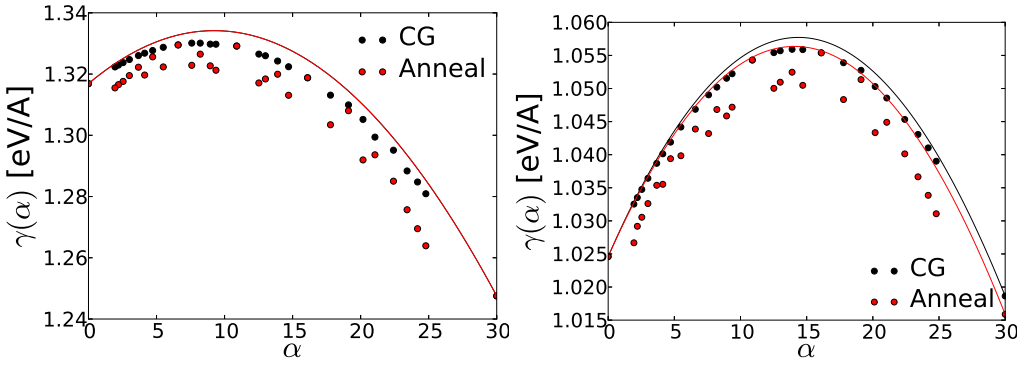

(a) AIREBO (b) LCBOP

Figure A.5: Edge energy of graphene edges for the AIREBO and the LCBOP potentials. The circles are the numerically measured values, while the lines are predictions from Eq. A.48. The relaxed edge configuration is calculated by two different methods, 'CG' or a conjugate gradient, and 'Anneal' or thermal annealing followed by few steps of steepest decent. It is interesting to see that the energies obtained by the annealing method show signs of the characteristic cusps at the high symmetry angles.

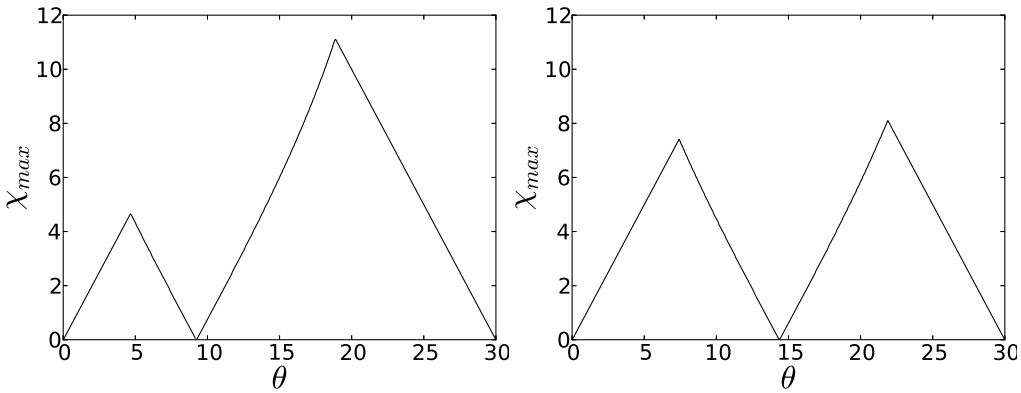

(a) AIREBO (b) LCBOP

Figure A.6: The maximum stable crack angle, χ_{max}, as a function of the orientation of the material axis θ (as predicted by Eqs. A.47).

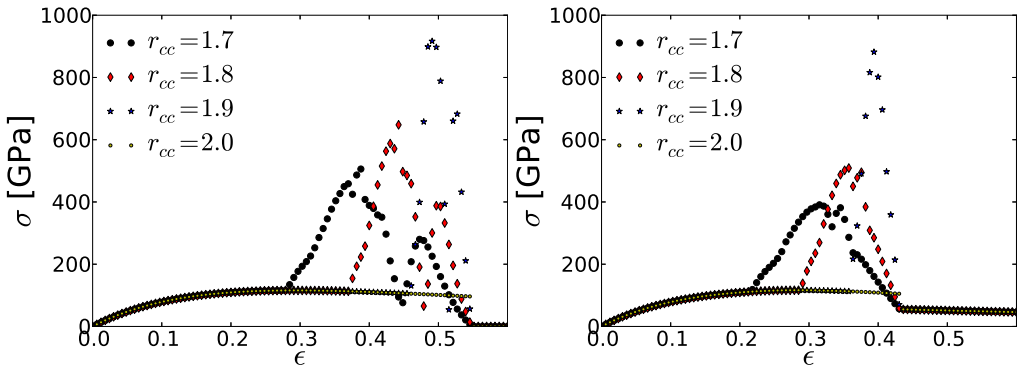

(a) Strain along the zigzag direction

(b) Strain along the armchair direction

Figure A.7: The stress strain curves for the AIREBO potential obtained by imposing a strain in a given direction and measuring the corresponding stress. The system is not relaxed after imposing the strain. Notice the unrealistic hardening at high strains, and the unreasonably high peak stress.

is based only on the edge energy, $\gamma(\cdot)$. The AIREBO potential has a tunable parameter r_{cc} which has no effect on the surface energy, and yet affects the crack behavior considerably, thereby debunking the theory. Figures A.7 and A.8 show the stress response of the AIREBO potential obtained by imposing a strain along the zigzag or the armchair direction and measuring the stress needed to hold the deformation. Notice that this behavior depends considerably on the parameter r_{cc}, and that there is a discontinuity in the behavior for $r_{cc} = 2.0$ (which is expected since the potential has a term with $r_{cc} - 2$ as the denominator). Also notice that the peak stress in the zigzag direction is much higher than that in the armchair direction. This indicates that the AIREBO potential is perhaps stronger in the zigzag direction (thus making it hard to create an armchair surface), and will perhaps favor cracks that grow along a zigzag surface. Figure A.9 shows the corresponding curves for the LCBOP potential. Notice that the LCBOP potential is much more isotropic in the sense that the peak stress in both directions is roughly the same.

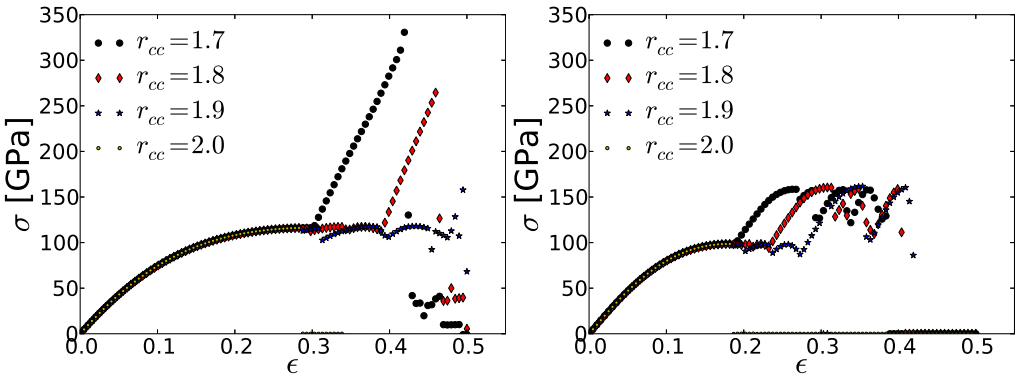

(a) Strain along the zigzag direction (b) Strain along the armchair direction

Figure A.8: The stress strain curves for the AIREBO potential obtained by imposing a strain in a given direction and measuring the corresponding stress. The system is relaxed after imposing the strain. Notice again the hardening at high strain.

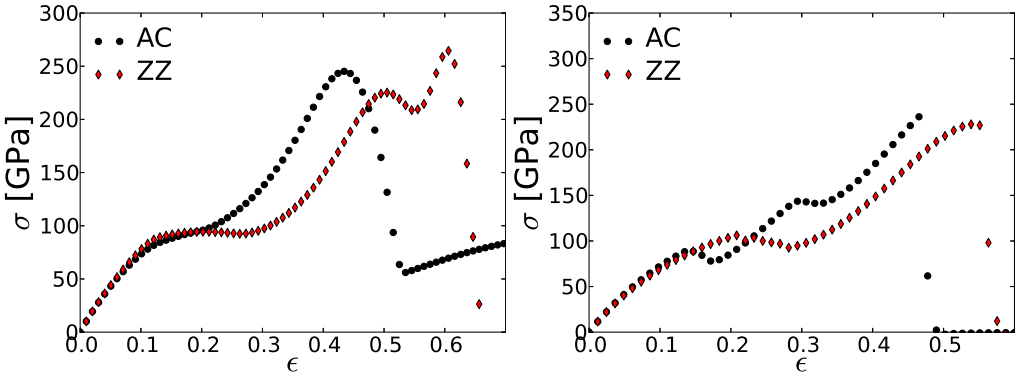

(a) Cell not relaxed after straining (b) Cell relaxed after straining

Figure A.9: The stress strain curves for the LCBOP potential obtained by imposing a strain in a given direction and measuring the corresponding stress. The system is relaxed after imposing the strain.

Figure A.10 shows the crack paths for various configurations for the AIREBO potential with $r_{cc} = 2.0$. It is clear that at this parameter value the cracks always grow along the zigzag direction. This is in violation of the predictions of the surface energy based theory. It is worth mentioning that while setting $r_{cc} = 2.0$ makes the potential brittle, leading to sharp cracks, it is perhaps objectionable on theoretical grounds since it introduces a discontinuity in the potential. However, choosing other values of the parameter leads to unrealistic behavior, such as that shown in figure A.11.

Figure A.12 shows the observed crack paths for the LCBOP potential. It is evident that thermal effects play a significant role in determining the crack path. The cracks grow straight at $T = 300$K, regardless of the lattice orientation, while at 10K they tend to grow along the zigzag axis for θ up to 15°, and straight otherwise. The dependence of crack growth direction on temperature will be investigated in a future paper.

(a) $\theta = 0°$ (b) $\theta = 8°$ (c) $\theta = 15°$ (d) $\theta = 23°$ (e) $\theta = 30°$

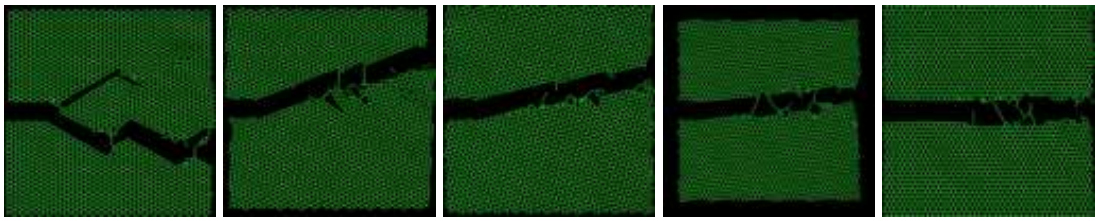

(f) $\theta = 0°$ (g) $\theta = 8°$ (h) $\theta = 15°$ (i) $\theta = 23°$ (j) $\theta = 30°$

Figure A.10: Crack paths for the AIREBO potential. Simulations a-e were done at $T = 10$K, while f-j were done at $T = 300$K. In all cases a strain of 10% was applied in the y-direction. It is clear that the cracks tend to propagate along the zigzag axis of graphene. At $\theta = 0°$ there are two equivalent zigzag directions, thus the crack tends to oscillate for configurations of low θ.

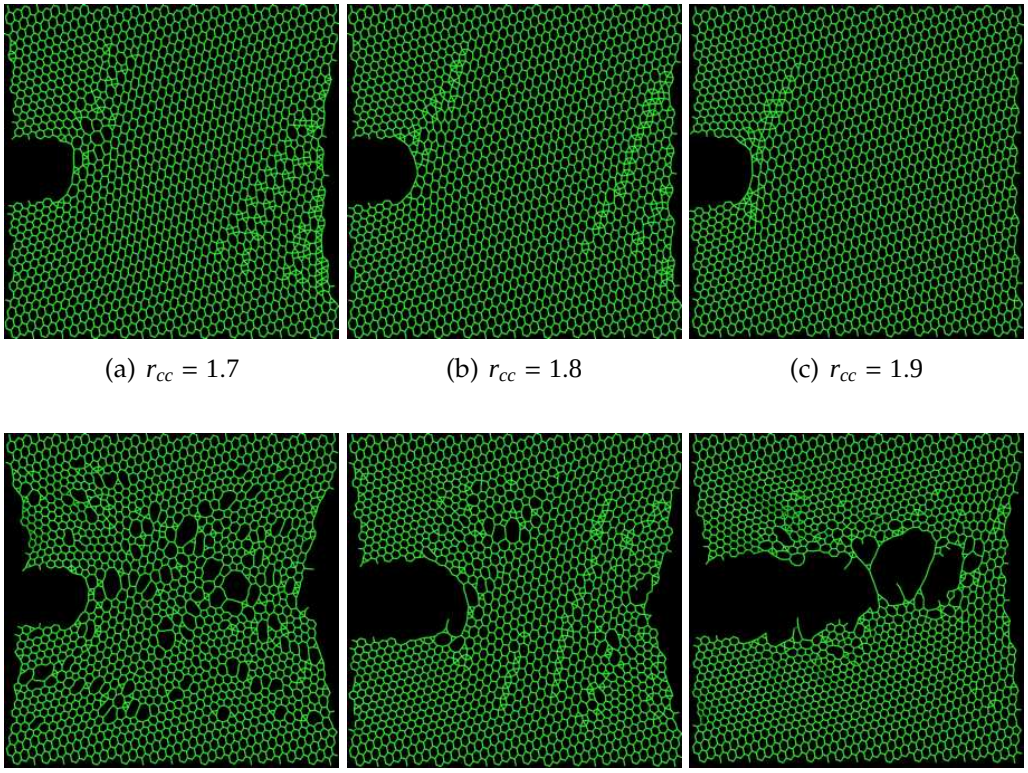

(a) r_{cc} = 1.7 (b) r_{cc} = 1.8 (c) r_{cc} = 1.9

(d) r_{cc} = 1.7 (e) r_{cc} = 1.8 (f) r_{cc} = 1.9

Figure A.11: Crack paths for the AIREBO potential at varying r_{cc}. Simulations a-c were done at T = 10K, while d-f were done at T = 300K. In all cases a strain of 40% was applied in the y-direction, and $\theta = 15^{\circ}$. Notice how the graphene sheet is able to withstand such a high strain by blunting the crack tip and relieving the stress via local plastic rearrangement of atoms

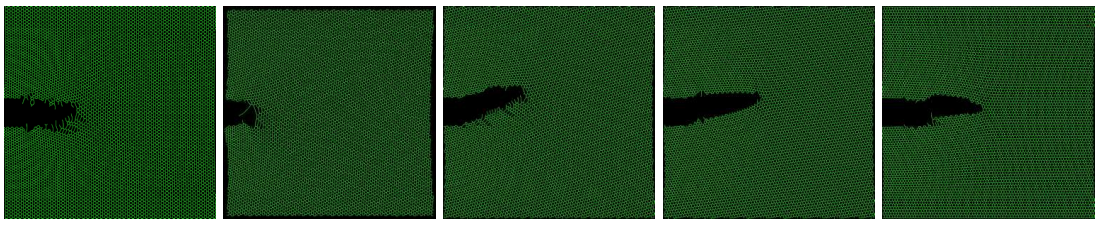

(a) $\theta = 0°$ (b) $\theta = 8°$ (c) $\theta = 15°$ (d) $\theta = 23°$ (e) $\theta = 30°$

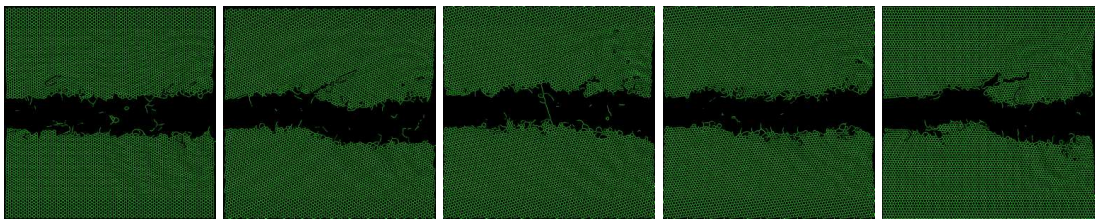

(f) $\theta = 0°$ (g) $\theta = 8°$ (h) $\theta = 15°$ (i) $\theta = 23°$ (j) $\theta = 30°$

Figure A.12: Crack paths for the LCBOP potential. Simulations a-e were done at $T = 10$K, while f-j were done at $T = 300$K. Notice the fact that for $T = 300$K all cracks grow straight.

BIBLIOGRAPHY

[1] S. M. Ross. *Applied probability models with optimization applications*. Courier Dover Publications, 1970.

[2] G. Casella and R. L. Berger. *Statistical inference*, volume 70. Duxbury Press Belmont, CA, 1990.

[3] S. I. Resnick. *Extreme values, regular variation and point processes*. Springer Verlag, New York, 2007.

[4] M. R. Leadbetter, G. Lindgren, and H. Rootzén. *Extremes and related properties of random sequences and processes*, volume 11. Springer Verlag, 1983.

[5] A. T. Zehnder. *Fracture Mechanics*, volume 62 of *Lecture Notes in Applied and Computational Mechanics*. Springer Verlag, New York, 2012.

[6] D. Gross and T. Seelig. *Fracture mechanics: with an introduction to micromechanics*. Springer, 2011.

[7] J. Cardy. *Scaling and renormalization in statistical physics*, volume 5. Cambridge University Press, 1996.

[8] J. P. Sethna. *Statistical mechanics: entropy, order parameters, and complexity*. Oxford University Press Oxford, 2006.

[9] A. Hansen and J. Schmittbuhl. Origin of the universal roughness exponent of brittle fracture surfaces: Stress-weighted percolation in the damage zone. *Phys. Rev. Lett.*, 90(4), 2003.

[10] A. A. Griffith. The phenomena of rupture and flow in solids. *Philosophical Transactions of the Royal Society of London. Series A, Containing Papers of a Mathematical or Physical Character*, 221:163–198, 1920.

[11] F. T. Peirce. Tensile tests for cotton yarns. *Journal of the Textile Institute*, 17:T355–368, 1926.

[12] C. E. Inglis. Stresses in a plate due to the presence of cracks and sharp corners. *Transactions of the Institution of Naval Architects*, XLIV:219–241, 1913.

[13] H. M. Westergaard. Bearing pressure and cracks. *Journal of Applied Mechanics*, 6:A 49–53, 1939.

[14] N. I. Muskhelishvili and J. R. M. Radok. *Some basic problems of the mathematical theory of elasticity*, volume 15. Cambridge University Press, 1953.

[15] G. R. Irwin. Analysis of stresses and strains near the end of a crack traversing a plate. *Journal of Applied Mechanics*, 24:361–364, 1957.

[16] G. R. Irwin and J. A. Kies. Fracturing and fracture dynamics. *Welding Journal Research Supplement*, 38:95–96, 1952.

[17] G. R. Irwin. Linear fracture mechanics, fracture transition, and fracture control. *Engineering Fracture Mechanics*, 1(2):241–257, 1968.

[18] J. D. Eshelby. The force on an elastic singularity. *Philosophical Transactions of the Royal Society of London. Series A, Mathematical and Physical Sciences*, 244(877):87, 1951.

[19] J. D. Eshelby. The continuum theory of lattice defects. *Solid state physics*, 3:79–144, 1956.

[20] J. D. Eshelby. The determination of the elastic field of an ellipsoidal inclusion, and related problems. *Proceedings of the Royal Society of London. Series A, Mathematical and Physical Sciences*, pages 376–396, 1957.

[21] J. D. Eshelby. The elastic field outside an ellipsoidal inclusion. *Proceedings of the Royal Society of London. Series A, Mathematical and Physical Sciences*, pages 561–569, 1959.

[22] D. S. Dugdale. Yielding of steel sheets containing slits. *Journal of the Mechanics and Physics of Solids*, 8(2):100 – 104, 1960.

[23] G. I. Barenblatt. The mathematical theory of equilibrium cracks in brittle fracture. *Advances in applied mechanics*, 7(55-129):104, 1962.

[24] B. A. Bilby, A. H. Cottrell, and K. H. Swinden. The spread of plastic yield from a notch. *Proceedings of the Royal Society of London. Series A. Mathematical and Physical Sciences*, 272(1350):304, 1963.

[25] A. Hillerborg, M. Modéer, and P. E. Petersson. Analysis of crack formation

and crack growth in concrete by means of fracture mechanics and finite elements. *Cement and concrete research*, 6(6):773–781, 1976.

[26] A. Needleman. A continuum model for void nucleation by inclusion debonding. *Journal of Applied Mechanics*, 54:525, 1987.

[27] X. P. Xu and A. Needleman. Numerical simulations of fast crack growth in brittle solids. *Journal of the Mechanics and Physics of Solids*, 42(9):1397–1434, 1994.

[28] G. T. Camacho and M. Ortiz. Computational modelling of impact damage in brittle materials. *International Journal of solids and structures*, 33(20-22):2899–2938, 1996.

[29] M. Elices, G. V. Guinea, J. Gomez, and J. Planas. The cohesive zone model: advantages, limitations and challenges. *Engineering fracture mechanics*, 69(2):137–163, 2002.

[30] N. Chandra, H. Li, C. Shet, and H. Ghonem. Some issues in the application of cohesive zone models for metal–ceramic interfaces. *International Journal of Solids and Structures*, 39(10):2827–2855, 2002.

[31] M. Ohnaka and T. Yamashita. A cohesive zone model for dynamic shear faulting based on experimentally inferred constitutive relation and strong motion source parameters. *Journal of Geophysical Research*, 94(B4):4089–4104, 1989.

[32] R. De Borst. Numerical aspects of cohesive-zone models. *Engineering fracture mechanics*, 70(14):1743–1757, 2003.

[33] H. Yuan, G. Lin, and A. Cornec. Verification of a cohesive zone model for ductile fracture. *Journal of engineering materials and technology*, 118:192, 1996.

[34] V. R. Coffman and J. P. Sethna. Grain boundary energies and cohesive strength as a function of geometry. *Physical Review B*, 77(14):144111, 2008.

[35] V. R. Coffman, J. P. Sethna, G. Heber, M. Liu, A. Ingraffea, N. P. Bailey, and E. I. Barker. A comparison of finite element and atomistic modelling of fracture. *Modelling and Simulation in Materials Science and Engineering*, 16:065008, 2008.

[36] J. R. Rice. A path independent integral and the approximate analysis of strain concentration by notches and cracks. *Journal of Applied Mechanics*, 35:379, 1968.

[37] J. R. Rice. Mathematical analysis in the mechanics of fracture. *Fracture: an advanced treatise*, 2:191–311, 1968.

[38] K. K. Lo. Analysis of branched cracks. *ASME, Transactions, Journal of Applied Mechanics*, 45:797–802, 1978.

[39] K. Hayashi and S. Nemat-Nasser. Energy release rate and crack kinking. *International Journal of Solids and Structures*, 17(1):107 – 114, 1981.

[40] J. Weertman. *Dislocation based fracture mechanics*. World Scientific Publishing Company, 1996.

[41] L. B. Freund. Crack propagation in an elastic solid subjected to general loadingi. constant rate of extension. *Journal of the Mechanics and Physics of Solids*, 20(3):129 – 140, 1972.

[42] P. A. Mataga, L. B. Freund, and J. W. Hutchinson. Crack tip plasticity in dynamic fracture. *Journal of Physics and Chemistry of Solids*, 48(11):985 – 1005, 1987.

[43] L. B. Freund. *Dynamic fracture mechanics*. Cambridge University Press, 1998.

[44] J. A. Kallivayalil, C. Y. Hui, and A. T. Zehnder. A method for thermo-mechanical analysis of steady state dynamic crack growth. *International Journal of Solids and Structures*, 33(13):1867 – 1889, 1996.

[45] H. Henry and H. Levine. Dynamic instabilities of fracture under biaxial strain using a phase field model. *Phys. Rev. Lett.*, 93:105504, Sep 2004.

[46] E. Weinan and Z. Huang. A dynamic atomisticcontinuum method for the simulation of crystalline materials. *Journal of Computational Physics*, 182(1):234 – 261, 2002.

[47] N. F. Mott. Brittle fracture in mild steel plates. *Engineering*, 165:16–18, 1948.

[48] N. F. Mott. Fragmentation of shell cases. *Proceedings of the Royal Society of London. Series A. Mathematical and Physical Sciences*, 189(1018):300–308, 1947.

[49] E. H. Yoffe. Lxxv. the moving griffith crack. *Philosophical Magazine Series 7*, 42(330):739–750, 1951.

[50] G. R. Irwin. Fracture dynamics. *Fracturing of metals*, 147:166, 1948.

[51] E. O. Hall. The brittle fracture of metals. *Journal of the Mechanics and Physics of Solids*, 1(4):227 – 233, 1953.

[52] E. Orowan. Energy criteria of fracture. *Welding Journal Research Supplement*, 34:157–160, 1955.

[53] A. A. Wells and D. Post. The dynamic stress distribution surrounding a running crack – a photoelastic analysis. *Proceedings of the SESA*, 16:69–92, 1958.

[54] A. A. Wells. Influence of residual stresses and metallurgical changes on low-stress brittle fracture in welded steel plates. *Welding Journal Research Supplement*, 40:182–192, 1961.

[55] C. F. Tipper. *The brittle fracture story*. University Press Cambridge, 1962.

[56] K. Ravi-Chandar and W. G. Knauss. An experimental investigation into dynamic fracture: I. crack initiation and arrest. *International Journal of Fracture*, 25:247–262, 1984. 10.1007/BF00963460.

[57] K. Ravi-Chandar and W. G. Knauss. An experimental investigation into dynamic fracture: Ii. microstructural aspects. *International Journal of Fracture*, 26:65–80, 1984. 10.1007/BF01152313.

[58] K. Ravi-Chandar and W. G. Knauss. An experimental investigation into dynamic fracture: Iii. on steady-state crack propagation and crack branching. *International Journal of Fracture*, 26:141–154, 1984. 10.1007/BF01157550.

[59] K. Ravi-Chandar and W. G. Knauss. An experimental investigation into dynamic fracture: Iv. on the interaction of stress waves with propagating cracks. *International Journal of Fracture*, 26:189–200, 1984. 10.1007/BF01140627.

[60] J. Fineberg and M. Marder. Instability in dynamic fracture. *Physics Reports*, 313(12):1 – 108, 1999.

[61] M. Marder and S. Gross. Origin of crack tip instabilities. *Journal of the Mechanics and Physics of Solids*, 43(1):1 – 48, 1995.

[62] D. Holland and M. Marder. Ideal brittle fracture of silicon studied with molecular dynamics. *Phys. Rev. Lett.*, 80:746–749, Jan 1998.

[63] M. Marder and X. Liu. Instability in lattice fracture. *Phys. Rev. Lett.*, 71:2417–2420, Oct 1993.

[64] J. Fineberg, S. P. Gross, M. Marder, and H. L. Swinney. Instability in dynamic fracture. *Phys. Rev. Lett.*, 67:457–460, Jul 1991.

[65] J. Fineberg, S. P. Gross, M. Marder, and H. L. Swinney. Instability in the propagation of fast cracks. *Phys. Rev. B*, 45:5146–5154, Mar 1992.

[66] S. P. Gross, J. Fineberg, M. Marder, W. D. McCormick, and H. L. Swinney. Acoustic emissions from rapidly moving cracks. *Phys. Rev. Lett.*, 71:3162–3165, Nov 1993.

[67] E. Sharon, S. P. Gross, and J. Fineberg. Local crack branching as a mechanism for instability in dynamic fracture. *Phys. Rev. Lett.*, 74:5096–5099, Jun 1995.

[68] E. Sharon and J. Fineberg. Microbranching instability and the dynamic fracture of brittle materials. *Phys. Rev. B*, 54:7128–7139, Sep 1996.

[69] E. Sharon, S. P. Gross, and J. Fineberg. Energy dissipation in dynamic fracture. *Phys. Rev. Lett.*, 76:2117–2120, Mar 1996.

[70] J. A. Hauch, D. Holland, M. P. Marder, and H. L. Swinney. Dynamic fracture in single crystal silicon. *Phys. Rev. Lett.*, 82:3823–3826, May 1999.

[71] E. Sharon and J. Fineberg. Confirming the continuum theory of dynamic brittle fracture for fast cracks. *Nature*, 397(6717):333–335, 1999.

[72] S. Ramanathan and D. S. Fisher. Dynamics and instabilities of planar tensile cracks in heterogeneous media. *Phys. Rev. Lett.*, 79:877–880, Aug 1997.

[73] S. Ramanathan, D. Ertaş, and D. S. Fisher. Quasistatic crack propagation in heterogeneous media. *Phys. Rev. Lett.*, 79:873–876, Aug 1997.

[74] S. Ramanathan and D. S. Fisher. Onset of propagation of planar cracks in heterogeneous media. *Phys. Rev. B*, 58:6026–6046, Sep 1998.

[75] E. Bouchaud, J. Bouchaud, D. Fisher, S. Ramanathan, and J. Rice. Can crack front waves explain the roughness of cracks? *Journal of the Mechanics and Physics of Solids*, 50(8):1703 – 1725, 2002.

[76] B. Mills, M. McLean, and E. Hondros. Surface-energy anisotropy of 3 percent si-fe. *Phil. Mag.*, 27(2):361–368, 1973.

[77] F. F. Abraham. *Computer Simulation in Materials Science*. Kluwer Publishing, The Netherlands, 1996.

[78] E. P. George, W. D. Porter, H. M. Henson, W. C. Oliver, and B. F. Oliver. Cleavage fracture in an Al3Ti-based alloy having the Ll2 structure. *Journal of Materials Research*, 4(01):78–84, 1989.

[79] F. F. Abraham. Dynamics of brittle fracture with variable elasticity. *Phys. Rev. Lett.*, 77:869–872, Jul 1996.

[80] R. Pérez and P. Gumbsch. Directional anisotropy in the cleavage fracture of silicon. *Phys. Rev. Lett.*, 84:5347–5350, Jun 2000.

[81] A. George and G. Michot. Dislocation loops at crack tips: nucleation and growth an experimental study in silicon. *Materials Science and Engineering: A*, 164(12):118 – 134, 1993.

[82] B. Cotterell and J. R. Rice. Slightly curved or kinked cracks. *International Journal of Fracture*, 16:155–169, 1980.

[83] B. L. Karihaloo, L. M. Keer, and S. Nemat-Nasser. Crack kinking under nonsymmetric loading. *Engineering Fracture Mechanics*, 13(4):879 – 888, 1980.

[84] Y. Sumi, S. Nemat-Nasser, and L. M. Keer. On crack path stability in a finite body. *Engineering Fracture Mechanics*, 22(5):759 – 771, 1985.

[85] H. Gao and C. Cheng-Hsin. Slightly curved or kinked cracks in

anisotropic elastic solids. *International Journal of Solids and Structures*, 29(8):947 – 972, 1992.

[86] M. Y. He and J. W. Hutchinson. Kinking of a crack out of an interface. *Journal of Applied Mechanics*, 56:270, 1989.

[87] M. Y. He, A. Bartlett, A. G. Evans, and J. W. Hutchinson. Kinking of a crack out of an interface: Role of in-plane stress. *Journal of the American Ceramic Society*, 74(4):767–771, 1991.

[88] A. G. Evans, B. J. Dalgleish, M. He, and J. W. Hutchinson. On crack path selection and the interface fracture energy in bimaterial systems. *Acta Metallurgica*, 37(12):3249 – 3254, 1989.

[89] J. A. Hodgdon and J. P. Sethna. Derivation of a general three-dimensional crack-propagation law: A generalization of the principle of local symmetry. *Phys. Rev. B*, 47:4831–4840, Mar 1993.

[90] H. E. Daniels. The statistical theory of the strength of bundles of threads. I. *Proceedings of the Royal Society of London. Series A, Mathematical and Physical Sciences*, 183(995):405–435, 1945.

[91] S. L. Phoenix and H. M. Taylor. The asymptotic strength distribution of a general fiber bundle. *Advances in Applied Probability*, 5(2):200–216, 1973.

[92] S. L. Phoenix. Probabilistic strength analysis of fibre bundle structures. *Fibre Science and Technology*, 7(1):15–31, 1974.

[93] S. L. Phoenix. Probabilistic inter-fiber dependence and the asymptotic strength distribution of classic fiber bundles. *International Journal of Engineering Science*, 13(3):287–304, 1975.

[94] D. G. Harlow and S. L. Phoenix. The chain-of-bundles probability model for the strength of fibrous materials I: analysis and conjectures. *Journal of Composite Materials*, 12(2):195, 1978.

[95] D. G. Harlow and S. L. Phoenix. The chain-of-bundles probability model for the strength of fibrous materials II: A numerical study of convergence. *Journal of Composite Materials*, 12(3):314, 1978.

[96] S. L. Phoenix. Stochastic strength and fatigue of fiber bundles. *International Journal of Fracture*, 14(3):327–344, 1978.

[97] S. L. Phoenix. The asymptotic distribution for the time to failure of a fiber bundle. *Advances in applied probability*, 11(1):153–187, 1979.

[98] S. L. Phoenix. Statistical theory for the strength of twisted fiber bundles with applications to yarns and cables. *Textile Research Journal*, 49(7):407, 1979.

[99] S. L. Phoenix. Statistical aspects of failure of fibrous materials. *Composite Materials, Testing and Design*, page 455, 1979.

[100] D. G. Harlow and S. L. Phoenix. Bounds on the probability of failure of composite materials. *International Journal of Fracture*, 15(4):321–336, 1979.

[101] Z. F. Li, D. T. Grubb, and S. L. Phoenix. Fiber interactions in the multi-fiber composite fragmentation test. *Composites science and technology*, 54(3):251–266, 1995.

[102] P. M. Duxbury and P. L. Leath. Exactly solvable models of material breakdown. *Phys. Rev. B*, 49:12676–12687, May 1994.

[103] S. Pradhan, A. Hansen, and B. K. Chakrabarti. Failure processes in elastic fiber bundles. *Rev. Mod. Phys.*, 82:499–555, Mar 2010.

[104] L. De Arcangelis, S. Redner, and H. J. Herrmann. A random fuse model for breaking processes. *Journal de Physique Lettres*, 46(13):585–590, 1985.

[105] A. M. Freudenthal. Statistical approach to brittle fracture. *Fracture*, 2:591–619, 1968.

[106] A. S. Jayatilaka and K. Trustrum. Statistical approach to brittle fracture. *Journal of Materials Science*, 12(7):1426–1430, 1977.

[107] P. M. Duxbury, P. D. Beale, and P. L. Leath. Size effects of electrical breakdown in quenched random media. *Phys. Rev. Lett.*, 57(8):1052–1055, 1986.

[108] P. M. Duxbury, P. L. Leath, and P. D. Beale. Breakdown properties of quenched random systems: The random-fuse network. *Phys. Rev. B*, 36(1):367–380, Jul 1987.

[109] P. M. Duxbury and P. L. Leath. The failure distribution in percolation models of breakdown. *Journal of Physics A: Mathematical and General*, 20:L411, 1987.

[110] P. M. Duxbury, S. G. Kim, and P. L. Leath. Size effect and statistics of fracture in random materials. *Materials Science and Engineering: A*, 176(1-2):25–31, 1994.

[111] P. M. Duxbury and P. L. Leath. Failure probability and average strength of disordered systems. *Physical review letters*, 72(17):2805–2808, 1994.

[112] B. Kahng, G. G. Batrouni, S. Redner, L. de Arcangelis, and H. J. Herrmann. Electrical breakdown in a fuse network with random, continuously distributed breaking strengths. *Phys. Rev. B*, 37(13), 1988.

[113] W. A. Curtin and H. Scher. Brittle fracture in disordered materials: A spring network model. *Journal of Materials Research*, 5(3):535–553, 1990.

[114] W. A. Curtin and H. Scher. Analytic model for scaling of breakdown. *Phys. Rev. Lett.*, 67:2457–2460, Oct 1991.

[115] D. Lockner. The role of acoustic emission in the study of rock fracture. *International Journal of Rock Mechanics and Mining Sciences & Geomechanics Abstracts*, 30(7):883 – 899, 1993.

[116] A. Petri, G. Paparo, A. Vespignani, A. Alippi, and M. Costantini. Experimental evidence for critical dynamics in microfracturing processes. *Phys. Rev. Lett.*, 73:3423–3426, Dec 1994.

[117] A. Garcimartin, A. Guarino, L. Bellon, and S. Ciliberto. Statistical properties of fracture precursors. *Phys. Rev. Lett.*, 79:3202–3205, Oct 1997.

[118] A. Guarino, A. Garcimartn, and S. Ciliberto. An experimental test of the critical behaviour of fracture precursors. *The European Physical Journal B - Condensed Matter and Complex Systems*, 6(1):13–24, 1998.

[119] C. Maes, A. Van Moffaert, H. Frederix, and H. Strauven. Criticality in creep experiments on cellular glass. *Phys. Rev. B*, 57:4987–4990, Mar 1998.

[120] L. I. Salminen, A. I. Tolvanen, and M. J. Alava. Acoustic emission from paper fracture. *Phys. Rev. Lett.*, 89:185503, Oct 2002.

[121] A. Hansen and P. C. Hemmer. Burst avalanches in bundles of fibers: Local versus global load-sharing. *Physics Letters A*, 184(6):394 – 396, 1994.

[122] F. Kun, S. Zapperi, and H. J. Herrmann. Damage in fiber bundle models. *The European Physical Journal B-Condensed Matter and Complex Systems*, 17(2):269–279, 2000.

[123] R. C. Hidalgo, F. Kun, and H. J. Herrmann. Bursts in a fiber bundle model with continuous damage. *Physical Review E*, 64(6):66122, 2001.

[124] S. Pradhan and B. K. Chakrabarti. Precursors of catastrophe in the Bak-Tang-Wiesenfeld, Manna, and random-fiber-bundle models of failure. *Physical Review E*, 65(1):16113, 2001.

[125] S. Pradhan, P. Bhattacharyya, and B. K. Chakrabarti. Dynamic critical behavior of failure and plastic deformation in the random fiber bundle model. *Physical Review E*, 66(1):16116, 2002.

[126] P. Bhattacharyya, S. Pradhan, and B. K. Chakrabarti. Phase transition in fiber bundle models with recursive dynamics. *Physical Review E*, 67(4):46122, 2003.

[127] S. Pradhan and B. K. Chakrabarti. Failure Properties of Fiber Bundle Models. *International Journal of Modern Physics B*, 17:5565–5581, 2003.

[128] S. Pradhan, B. K. Chakrabarti, and A. Hansen. Crossover behavior in a mixed-mode fiber bundle model. *Physical Review E*, 71(3):36149, 2005.

[129] S. Pradhan, A. Hansen, and P. C. Hemmer. Crossover behavior in burst avalanches: Signature of imminent failure. *Physical review letters*, 95(12):125501, 2005.

[130] S. Pradhan and P. C. Hemmer. Energy bursts in fiber bundle models of composite materials. *Physical Review E*, 77(3):31138, 2008.

[131] Gilabert, A., Vanneste, C., Sornette, D., and Guyon, E. The random fuse network as a model of rupture in a disordered medium. *J. Phys. France*, 48(5):763–770, 1987.

[132] L. De Arcangelis, A. Hansen, H. J. Herrmann, and S. Roux. Scaling laws in fracture. *Physical Review B*, 40(1):877–880, 1989.

[133] A. Hansen, E. L. Hinrichsen, and S. Roux. Roughness of crack interfaces. *Physical review letters*, 66(19):2476–2479, 1991.

[134] A. Hansen, E. L. Hinrichsen, and S. Roux. Scale invariant disorder in fracture and related breakdown phenomena. *Phys. Rev. B*, 43:665, 1991.

[135] B. K. Chakrabarti and L. G. Benguigui. *Statistical physics of fracture and breakdown in disordered systems*. Oxford University Press, New York, 1997.

[136] S. Zapperi, P. Ray, H. E. Stanley, and A. Vespignani. First-order transition in the breakdown of disordered media. *Phys. Rev. Lett.*, 78(8), 1997.

[137] S. Zapperi, A. Vespignani, and H. E. Stanley. Plasticity and avalanche behaviour in microfracturing phenomena. *Nature*, 388(6643):658–659, 1997.

[138] V. I. Raisanen, M. J. Alava, and R. M. Nieminen. Fracture of three-dimensional fuse networks with quenched disorder. *Physical Review B*, 58(21):14288–14295, 1998.

[139] S. Zapperi, P. Ray, H. E. Stanley, and A. Vespignani. Avalanches in breakdown and fracture processes. *Physical Review E*, 59(5):5049–5057, 1999.

[140] S. Zapperi, P. Ray, H. E. Stanley, and A. Vespignani. Analysis of damage clusters in fracture processes. *Physica A: Statistical Mechanics and its Applications*, 270(1-2):57–62, 1999.

[141] S. Zapperi, H. J. Herrmann, and S. Roux. Planar cracks in the fuse model. *The European Physical Journal B-Condensed Matter and Complex Systems*, 17(1):131–136, 2000.

[142] D. Sornette and C. Vanneste. Dynamics and memory effects in rupture of thermal fuse networks. *Physical review letters*, 68(5):612–615, 1992.

[143] P. K. V. V. Nukala, S. Šimunović, and S. Zapperi. Percolation and localization in the random fuse model. *Journal of Statistical Mechanics: Theory and Experiment*, 2004:P08001, 2004.

[144] S. Zapperi, P. K. V. V. Nukala, and S. Šimunović. Crack roughness and avalanche precursors in the random fuse model. *Physical Review E*, 71(2):26106, 2005.

[145] P. K. V. V. Nukala, S. Zapperi, and S. Šimunović. Statistical properties of fracture in a random spring model. *Physical Review E*, 71(6):66106, 2005.

[146] S. Zapperi, P. K. V. V. Nukala, and S. Simunovic. Crack avalanches in the three-dimensional random fuse model. *Physica A: Statistical Mechanics and its Applications*, 357(1):129–133, 2005.

[147] J. V. Andersen, D. Sornette, and K.-t. Leung. Tricritical behavior in rupture induced by disorder. *Phys. Rev. Lett.*, 78:2140–2143, Mar 1997.

[148] D. Sornette and J. V. Andersen. Scaling with respect to disorder in time-to-failure. *The European Physical Journal B - Condensed Matter and Complex Systems*, 1(3):353–357, 1998.

[149] A. Johansen and D. Sornette. Critical ruptures. *The European Physical Journal B - Condensed Matter and Complex Systems*, 18(1):163–181, 2000.

[150] S. Gluzman and D. Sornette. Self-consistent theory of rupture by progressive diffuse damage. *Phys. Rev. E*, 63:066129, May 2001.

[151] W. Weibull. *A statistical theory of the strength of materials*. Generalstabens litografiska anstalts f
"orlag, 1939.

[152] W. Weibull. A statistical distribution function of Wide Applicability. *Journal of applied mechanics*, pages 293–297, 1951.

[153] R. A. Hunt and L. N. McCartney. A new approach to Weibull's statistical theory of brittle fracture. *International Journal of Fracture*, 15(4):365–375, 1979.

[154] M. Sutcu. Weibull statistics applied to fiber failure in ceramic composites and work of fracture. *Acta Metallurgica*, 37(2):651–661, 1989.

[155] F. Minami, A. Bruckner-Foit, D. Munz, and B. Trolldenier. Estimation procedure for the Weibull parameters used in the local approach. *International Journal of Fracture*, 54(3):197–210, 1992.

[156] L. Y. Chao and D. K. Shetty. Extreme-Value Statistics Analysis of Fracture Strengths of a Sintered Silicon Nitride Failing from Pores. *Journal of the American Ceramic Society*, 75(8):2116–2124, 1992.

[157] D. W. Nicholson and P. Ni. Extreme value probabilistic theory for mixed-mode brittle fracture. *Engineering fracture mechanics*, 58(1-2):121–132, 1997.

[158] I. J. Beyerlein and S. L. Leigh Phoenix. Statistics of fracture for an elastic notched composite lamina containing Weibull fibers–Part I. Features from Monte-Carlo simulation. *Engineering Fracture Mechanics*, 57(2-3):241–265, 1997.

[159] X. Gao, C. Ruggieri, and R. H. Dodds. Calibration of Weibull stress parameters using fracture toughness data. *International Journal of Fracture*, 92(2):175–200, 1998.

[160] X. Gao, R. H. D. Jr, R. L. Tregoning, J. A. Joyce, and R. E. Link. A weibull stress model to predict cleavage fracture in plates containing surface cracks. *Fatigue & Fracture of Engineering Materials & Structures*, 22(6):481–493, 1999.

[161] C. Lu, R. Danzer, and F. D. Fischer. Fracture statistics of brittle materials: Weibull or normal distribution. *Physical Review E*, 65(6):67102, 2002.

[162] H. D. Espinosa, B. Peng, B. C. Prorok, N. Moldovan, O. Auciello, J. A. Carlisle, D. M. Gruen, and D. C. Mancini. Fracture strength of ultrananocrystalline diamond thin filmsidentification of Weibull parameters. *Journal of Applied Physics*, 94:6076, 2003.

[163] R. Danzer. Some notes on the correlation between fracture and defect statistics: Are Weibull statistics valid for very small specimens? *Journal of the European Ceramic Society*, 26(15):3043–3049, 2006.

[164] R. H. Doremus. Fracture statistics: A comparison of the normal, Weibull, and Type I extreme value distributions. *Journal of Applied Physics*, 54(1):193–198, 2009.

[165] A. Evans. Statistical aspects of cleavage fracture in steel. *Metallurgical and Materials Transactions A*, 14:1349–1355, 1983.

[166] T. Lin, A. G. Evans, and R. O. Ritchie. Stochastic modeling of the independent roles of particle size and grain size in transgranular cleavage fracture. *Metallurgical And Materials Transactions A*, 18(5):641 – 651, 1987.

[167] F. Beremin, A. Pineau, F. Mudry, J. C. Devaux, Y. D'Escatha, and P. Ledermann. A local criterion for cleavage fracture of a nuclear pressure vessel steel. *Metallurgical and Materials Transactions A*, 14:2277–2287, 1983.

[168] T. Lin, A. G. Evans, and R. O. Ritchie. A statistical model of brittle fracture

by transgranular cleavage. *Journal of the Mechanics and Physics of Solids*, 34(5):477 – 497, 1986.

[169] T. Lin, A. G. Evans, and R. O. Ritchie. Statistical analysis of cleavage fracture ahead of sharp cracks and rounded notches. *Acta Metallurgica*, 34(11):2205 – 2216, 1986.

[170] L. Xia and C. F. Shih. Ductile crack growthiii. transition to cleavage fracture incorporating statistics. *Journal of the Mechanics and Physics of Solids*, 44(4):603 – 639, 1996.

[171] F. Mudry. A local approach to cleavage fracture. *Nuclear Engineering and Design*, 105(1):65 – 76, 1987.

[172] D. A. Curry and J. F. Knott. Effect of microstructure on cleavage fracture toughness of quenched and tempered steels. *Metal Science*, 13(6):341–345, 1979.

[173] A. J. Horn and A. H. Sherry. Prediction of cleavage fracture from non-sharp defects using the weibull stress based toughness scaling model. *International Journal of Pressure Vessels and Piping*, 87(12):670 – 680, 2010.

[174] J. Faleskog, M. Kroon, and H. Oberg. A probabilistic model for cleavage fracture with a length scaleparameter estimation and predictions of stationary crack experiments. *Engineering Fracture Mechanics*, 71(1):57 – 79, 2004.

[175] R. A. Fisher and L. H. C. Tippett. Limiting forms of the frequency distribution of the largest or smallest member of a sample. *Mathematical Proceedings of the Cambridge Philosophical Society*, 24:180–190, 3 1928.

[176] B. Gnedenko. Sur la distribution limite du terme maximum d'une serie aleatoire. *Annals of Mathematics*, 44(3):pp. 423–453, 1943.

[177] B. Epstein. Application of the theory of extreme values in fracture problems. *Journal of the American Statistical Association*, 43(243):403–412, 1948.

[178] E. J. Gumbel and J. Lieblein. *Statistical theory of extreme values and some practical applications: A series of lectures*. U.S. Govt. Print Office, 1954.

[179] E. J. Gumbel. *Statistics of extremes*. Columbia University Press, New York, 1958.

[180] A. M. Freudenthal and E. J. Gumbel. On the statistical interpretation of fatigue tests. *Proceedings of the Royal Society of London. Series A, Mathematical and Physical Sciences*, 216(1126):309–332, 1953.

[181] S. I. Resnick. Tail equivalence and its applications. *Journal of Applied Probability*, 8(1):136–156, 1971.

[182] C. W. Anderson. Super-slowly varying functions in extreme value theory. *Journal of the Royal Statistical Society. Series B (Methodological)*, 40(2):197–202, 1978.

[183] L. de Haan and S. I. Resnick. Second-order regular variation and rates of convergence in extreme-value theory. *The Annals of Probability*, 24(1):97–124, 1996.

[184] G. Györgyi, N. R. Moloney, K. Ozogány, and Z. Rácz. Finite-size scaling in extreme statistics. *Phys. Rev. Lett.*, 100(21):210601, May 2008.

[185] G. Györgyi, N. R. Moloney, K. Ozogány, Z. Rácz, and M. Droz. Renormalization-group theory for finite-size scaling in extreme statistics. *Phys. Rev. E*, 81(4):041135, Apr 2010.

[186] E. Bertin and M. Clusel. Generalized extreme value statistics and sum of correlated variables. *Journal of Physics A: Mathematical and General*, 39(24):7607, 2006.

[187] M. J. Alava, P. K. V. V. Nukala, and S. Zapperi. Statistical models of fracture. *Advances in Physics*, 55(3):349–476, 2006.

[188] S. L. Phoenix and I. J. Beyerlein. Distributions and size scalings for strength in a one-dimensional random lattice with load redistribution to nearest and next-nearest neighbors. *Phys. Rev. E*, 62(2):1622–1645, Aug 2000.

[189] P. D. Beale and P. M. Duxbury. Theory of dielectric breakdown in metal-loaded dielectrics. *Phys. Rev. B*, 37(6):2785–2791, Feb 1988.

[190] S. L. Phoenix, M. Ibnabdeljalil, and C.-Y. Hui. Size effects in the distribution for strength of brittle matrix fibrous composites. *International Journal of Solids and Structures*, 34(5):545 – 568, 1997. (See Fig. 6).

[191] A. Sharoni, J. G. Ramírez, and I. K. Schuller. Multiple avalanches across

the metal-insulator transition of vanadium oxide nanoscaled junctions. *Phys. Rev. Lett.*, 101(2):026404, Jul 2008.

[192] Y. J. Chang, J. S. Yang, Y. S. Kim, D. H. Kim, T. W. Noh, D.-W. Kim, E. Oh, B. Kahng, and J.-S. Chung. Surface versus bulk characterizations of electronic inhomogeneity in a vo_2 thin film. *Phys. Rev. B*, 76(7):075118, Aug 2007.

[193] M. M. Qazilbash, M. Brehm, G. O. Andreev, A. Frenzel, P.-C. Ho, B.-G. Chae, B.-J. Kim, S. J. Yun, H.-T. Kim, A. V. Balatsky, O. G. Shpyrko, M. B. Maple, F. Keilmann, and D. N. Basov. Infrared spectroscopy and nano-imaging of the insulator-to-metal transition in vanadium dioxide. *Phys. Rev. B*, 79(7):075107, Feb 2009.

[194] J. Wu, Q. Gu, B. S. Guiton, N. P. de Leon, L. Ouyang, and H. Park. Strain-induced self organization of metalinsulator domains in single-crystalline vo2 nanobeams. *Nano Letters*, 6(10):2313–2317, 2006.

[195] T.-L. Wu, L. Whittaker, S. Banerjee, and G. Sambandamurthy. Temperature and voltage driven tunable metal-insulator transition in individual w_{x}v_{1-x}o_{2} nanowires. *Phy. Rev. B*, 83(7), 2011.

[196] M. Imada, A. Fujimori, and Y. Tokura. Metal insulator transitions. *Rev. Mod. Phys.*, 70:1039, 1998.

[197] L. Niemeyer, L. Pietronero, and H. J. Wiesmann. Fractal dimension of dielectric breakdown. *Phys. Rev. Lett.*, 52(12):1033–1036, 1984.

[198] T. Kikuzuki, R. Takahashi, and M. Lippmaa. Strained state dynamics in a vo_2 thin film. *Phys. Rev. B*, 82(14):144113, Oct 2010.

[199] M. M. Qazilbash, M. Brehm, B.-G. Chae, P.-C. Ho, G. O. Andreev, B.-J. Kim, S. J. Yun, A. V. Balatsky, M. B. Maple, F. Keilmann, H.-T. Kim, and D. N. Basov. Mott Transition in VO2 Revealed by Infrared Spectroscopy and Nano-Imaging. *Science*, 318(5857):1750–1753, 2007.

[200] B. Kim, Y. Lee, B. Chae, S. Yun, S. Oh, H. Kim, and Y. Lim. Temperature dependence of the first-order metal-insulator transition in vo[sub 2] and programmable critical temperature sensor. *Appl. Phys. Lett.*, 90(2):023515, 2007.

[201] M. Eckstein, T. Oka, and P. Werner. Dielectric breakdown of mott insula-

tors in dynamical mean-field theory. *Phys. Rev. Lett.*, 105(14):146404, Sep 2010.

[202] V. Eyert. The metal-insulator transitions of vo2: A band theoretical approach. *Annalen der Physik*, 11(9):650–704, 2002.

[203] M. B. Salamon and M. Jaime. The physics of manganites : Structure and transport. *Rev. Mod. Phys.*, 73:583, 2001.

[204] E. Dagotto, T. Hotta, and A. Moreo. Colossal magnetoresistant materials: the key role of phase separation. *Phys. Rep.*, 344:1, 2001.

[205] S. Papanikolaou *et al.* Universality of liquid-gas mott transitions at finite temperatures. *Phys. Rev. Lett.*, 100:026408, 2008.

[206] J.-N. Roux and D. Wilkinson. Resistance jumps in mercury injection in porous media. *Phys. Rev. A*, 37(10):3921–3926, May 1988.

[207] J. A. Blackman. A theory of conductivity in disordered resistor networks. *J. Phys. C: Solid State Phys.*, 9:2049, 1976.

[208] A. Mughal, L. Laurson, G. Durin, and S. Zapperi. Effect of dipolar interactions for domain-wall dynamics in magnetic thin films. *Magnetics, IEEE Transactions on*, 46(2):228–230, 2010.

[209] P. K. V. V. Nukala and S. Simunovic. An efficient algorithm for simulating fracture using large fuse networks. *J. Phys. A: Math. Gen.*, 36(45):11403–11412, 2003.

[210] F. Kagawa, K. Miyagawa, and K. Kanoda. Unconventional critical behaviour in a quasi-two-dimensional organic conductor. *Nature*, 436:534, 2005.

[211] J. Singleton and C. Mielke. Quasi-two-dimensional organic superconductors: a review. *Contemp. Phys.*, 43:63, 2002.

[212] P. Limelette *et al.* Universality and Critical Behavior at the Mott Transition. *Science*, 302(5642):89–92, 2003.

[213] S. Roux, A. Hansen, H. Herrmann, and E. Guyon. Rupture of heterogeneous media in the limit of infinite disorder. *Journal of Statistical Physics*, 52:237–244, 1988.

[214] D. Bonamy and E. Bouchaud. Failure of heterogeneous materials: A dynamic phase transition? *Physics Reports*, 498(1):1 – 44, 2011.

[215] P. C. Hemmer and A. Hansen. The distribution of simultaneous fiber failures in fiber bundles. *Journal of applied mechanics*, 59:909, 1992.

[216] M. J. Alava, P. K. V. V. Nukala, and S. Zapperi. Size effects in statistical fracture. *Journal of Physics D: Applied Physics*, 42(21):214012, 2009.

[217] Z. P. Bazant. Scaling theory for quasibrittle structural failure. *PNAS*, 101:13400, 2004.

[218] C. Manzato, A. Shekhawat, P. K. V. V. Nukala, M. J. Alava, J. P. Sethna, and S. Zapperi. Fracture strength of disordered media: Universality, interactions, and tail asymptotics. *Phys. Rev. Lett.*, 108:065504, Feb 2012.

[219] R. Otter. The multiplicative process. *Annals of Mathematical Statistics*, 49, 1949.

[220] J. P. Sethna, K. A. Dahmen, and C. R. Myers. Crackling noise. *Nature*, 410:242–250, 2001.

[221] A. Shekhawat, S. Papanikolaou, S. Zapperi, and J. P. Sethna. Dielectric breakdown and avalanches at nonequilibrium metal-insulator transitions. *Physical Review Letters*, 107(27):276401, 2011.

[222] W. G. Ellenbroek and X. Mao. Rigidity percolation on the square lattice. *EPL (Europhysics Letters)*, 96(5):54002, 2011.

[223] L. Ghivelder, R. S. Freitas, M. G. das Virgens, M. A. Continentino, H. Martinho, L. Granja, M. Quintero, G. Leyva., P. Levy, and F. Parisi. Abrupt field-induced transition triggered by magnetocaloric effect in phase-separated manganites. *Phys. Rev. B*, 69:214414, Jun 2004.

[224] S. Plimpton. Fast parallel algorithms for short-range molecular dynamics. *Journal of Computational Physics*, 117(1):1 – 19, 1995.

[225] S. J. Stuart, A. B. Tutein, and J. A. Harrison. A reactive potential for hydrocarbons with intermolecular interactions. *The Journal of Chemical Physics*, 112:6472, 2000.

[226] J. H. Los and A. Fasolino. Intrinsic long-range bond-order potential for carbon: Performance in monte carlo simulations of graphitization. *Phys. Rev. B*, 68:024107, Jul 2003.

[227] A. C. T. van Duin, S. Dasgupta, F. Lorant, and W. A. Goddard. Reaxff: a reactive force field for hydrocarbons. *The Journal of Physical Chemistry A*, 105(41):9396–9409, 2001.

[228] K. Chenoweth, A. C. T. van Duin, and W. A. Goddard. Reaxff reactive force field for molecular dynamics simulations of hydrocarbon oxidation. *The Journal of Physical Chemistry A*, 112(5):1040–1053, 2008. PMID: 18197648.

[229] A. Strachan, A. C. T. van Duin, D. Chakraborty, S. Dasgupta, and W. A. Goddard. Shock waves in high-energy materials: The initial chemical events in nitramine rdx. *Phys. Rev. Lett.*, 91:098301, Aug 2003.

[230] Y. Wei, J. Wu, H. Yin, X. Shi, R. Yang, and M. Dresselhaus. The nature of strength enhancement and weakening by pentagon–heptagon defects in graphene. *Nature Materials*, 11(9):759–763, 2012.

[231] Y. Liu, A. Dobrinsky, and B. I. Yakobson. Graphene edge from armchair to zigzag: The origins of nanotube chirality? *Phys. Rev. Lett.*, 105:235502, Dec 2010.